Title	Validity of the source term for the Fukushima Dai-ichi Nuclear Power Station accident estimated using local-scale atmospheric dispersion simulations to reproduce the large-scale atmospheric dispersion of ^{137}Cs
Author(s)	Kadowaki Masanao, Furuno Akiko, Nagai Haruyasu, Kawamura Hideyuki, Terada Hiroaki, Tsuzuki Katsunori, El-Asaad. H.
Citation	Journal of Environmental Radioactivity,237,p.106704_1-106704_18
Text Version	Published Journal Article
URL	https://jopss.jaea.go.jp/search/servlet/search?5071147
DOI	https://doi.org/10.1016/j.jenvrad.2021.106704
Right	

Journal of Environmental Radioactivity 237 (2021) 106704

Contents lists available at ScienceDirect

Journal of Environmental Radioactivity

journal homepage: www.elsevier.com/locate/jenvrad

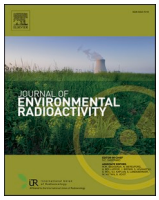

Validity of the source term for the Fukushima Dai-ichi Nuclear Power Station accident estimated using local-scale atmospheric dispersion simulations to reproduce the large-scale atmospheric dispersion of ^{137}Cs

Masanao Kadowaki *, Akiko Furuno, Haruyasu Nagai, Hideyuki Kawamura, Hiroaki Terada, Katsunori Tsuduki, Hamza El-Assad

Japan Atomic Energy Agency, 2-4 Shirakata, Tokai, Naka-gun, Ibaraki, 319-1195, Japan

ARTICLE INFO

Keywords:
Hemispheric-scale atmospheric dispersion
Fukushima Dai-ichi nuclear power station accident
137Cs
WSPEEDI-DB
Source term

ABSTRACT

The source term of ^{137}Cs from the Fukushima Dai-ichi Nuclear Power Station (FDNPS) accident was estimated from the results of local-scale atmospheric dispersion simulations and measurements. To confirm the source term's validity for reproducing the large-scale atmospheric dispersion of ^{137}Cs, this study conducted hemispheric-scale atmospheric and oceanic dispersion simulations. In the dispersion simulations, the atmospheric-dispersion database system Worldwide version of System for Prediction of Environmental Emergency Dose Information (WSPEEDI)-DB and oceanic dispersion model SEA-GEARN-FDM that were developed by the Japan Atomic Energy Agency were used. Compared with the air concentrations of ^{137}Cs measured by the Comprehensive Nuclear-Test-Ban Treaty Organization, overall, the WSPEEDI-DB simulations well reproduced the measurements, whereas the simulation results partly overestimated some measurements. Furthermore, the validity of the deposition of ^{137}Cs by WSPEEDI-DB was investigated using SEA-GEARN-FDM and concentrations of ^{137}Cs in seawater sampled from the North Pacific. Seawater concentrations of ^{137}Cs by the oceanic dispersion simulation, in which the deposition flux of ^{137}Cs by WSPEEDI-DB was used as input from the atmosphere to oceans, were statistically consistent to the measurement. However, the simulated seawater concentrations of ^{137}Cs were underestimated regionally in the North Pacific. Both the overestimation of air concentrations and underestimation of seawater concentrations could be attributed to the less amounts of ^{137}Cs deposition by less precipitation over the North Pacific. The overestimation and underestimation could be improved without contradiction between the air and seawater concentrations of ^{137}Cs using more realistic precipitation in atmospheric dispersion simulations. This shows that the source term validated in this study could reproduce the spatiotemporal distribution of ^{137}Cs from the FDNPS accident in both local and large-scale atmospheric dispersion simulations.

1. Introduction

The Great East Japan Earthquake on March 11, 2011, caused the accident at the Fukushima Daiichi Nuclear Power Station (FDNPS) of the Tokyo Electric Power Company. Consequently, substantial radioactive materials were released into the atmosphere and ocean. It is critical to find the source term in determining the environmental impact of a nuclear accident and its resultant radiological doses to the public. Therefore, the Japan Atomic Energy Agency (JAEA) has carried out atmospheric and oceanic dispersion simulations since the early stage of the accident, and has ongoingly estimated and updated the source term (Chino et al., 2011, 2016; Katata et al., 2012a, 2012b, 2015; Terada et al., 2012, 2020a; Kobayashi et al., 2013). In these studies, the Worldwide version of System for Prediction of Environmental Emergency Dose Information (WSPEEDI), developed by JAEA (Terada and Chino, 2008), was predominantly used except for oceanic simulations. The results of atmospheric dispersion simulations using WSPEEDI were validated by their comparison to measurement data for air concentrations and surface depositions of radioactive materials and air dose rate in the environment in Japan. In the report published by the United Nations Scientific Committee on the Effects of Atomic Radiation (UNSCEAR), the source term estimated by Terada et al. (2012) was used for evaluating

* Corresponding author.
E-mail address: kadowaki.masanao@jaea.go.jp (M. Kadowaki).

https://doi.org/10.1016/j.jenvrad.2021.106704
Received 15 March 2021; Received in revised form 13 July 2021; Accepted 14 July 2021

levels of radioactive material in the terrestrial environment and doses to the public where measurements did not exist (UNSCEAR , 2014).

Katata et al. (2015) successfully reproduced the local and regional deposition patterns of ^{137}Cs derived from airborne survey in Japan (Torii et al., 2013; MEXT, 2012). Unlike that study using local and regional scale simulations, several studies have estimated the source term and the environmental impact of released ^{137}Cs into the atmosphere based on global-scale atmospheric dispersion simulations (e.g., Stohl et al., 2012; Achim et al., 2014; Maki, 2015; Mészáros et al., 2015; Sarkar et al., 2017). Katata et al. (2015) also conducted the hemispheric-scale atmospheric dispersion simulation. The simulation results correlated well with the air concentrations of ^{137}Cs measured at the International Monitoring system (IMS) stations, which are part of the verification system of the Comprehensive Nuclear-Test-Ban Treaty Organization (CTBTO (2011). However, Katata et al. (2015) used a Hybrid Single Particle Lagrangian Integrated Trajectory model (HYSPLIT) (Draxler and Rolph, 2012), and the reproducibility of air concentrations and surface depositions of ^{137}Cs using the global-scale WSPEEDI simulations, was not investigated.

Mészáros et al. (2015) and Sarkar et al. (2017) independently conducted global-scale atmospheric dispersion simulations using the source term of Katata et al. (2015) and compared the results with the measurement data from IMS stations. Although both results agreed with air concentrations of ^{137}Cs measured at IMS stations, the reproducibility of ^{137}Cs surface deposition was not investigated because of a lack of surface deposition measurements, especially over the Pacific Ocean. To validate both air concentrations and surface depositions of ^{137}Cs obtained from simulations, JAEA conducted atmospheric dispersion simulations using WSPEEDI and oceanic dispersion simulations using the oceanic dispersion model SEA-GEARN-FDM (Kawamura et al., 2014, 2017). In Kawamura et al. (2014) and Kawamura et al. (2017), the deposition flux of ^{137}Cs calculated using WSPEEDI was used as inputs in the oceanic dispersion simulations. By comparing the measurements, concentrations of ^{137}Cs in sea surface water simulated using SEA-GEARN-FDM reasonably agreed with those sampled from the western North Pacific, whereas the simulated concentrations of ^{137}Cs were underestimated in the eastern North Pacific. This underestimation could be because of fewer amounts of transported ^{137}Cs, which were aerially released from FDNPS, to the eastern North Pacific.

Terada et al. (2020a) refined the source term estimated by Katata et al. (2015) using the atmospheric-dispersion database system simulations, WSPEEDI-DB (Terada et al., 2020b), and new monitoring data obtained from eastern Japan. In Terada et al. (2020a), objective analysis using Bayesian inference optimized the source term and atmospheric dispersion simulations. This optimization was conducted using measurements, such as air concentration, including newly disclosed hourly air concentrations of ^{137}Cs, surface deposition, and fallout. The hourly air concentrations of ^{137}Cs were derived by analyzing suspended particulate matter collected at air pollution monitoring stations in Japan (Oura et al., 2015; Tsuruta et al., 2018). Consequently, Terada et al. (2020a) successfully reproduced both the air concentrations of ^{137}Cs at the monitoring points and the surface deposition of ^{137}Cs by airborne monitoring in Japan. However, the validity of the source term by Terada et al. (2020a) remained unconfirmed in large-scale dispersion simulations.

In this study, we validate the source term by Terada et al. (2020a) in large-scale dispersion simulations. To achieve the validation, we conducted atmospheric dispersion simulations using WSPEEDI-DB with the source terms by Terada et al. (2020a) and Katata et al. (2015) and compared the simulated air concentrations of ^{137}Cs with measurements at the IMS stations. In addition, we validated the simulated ^{137}Cs deposition and concentrations of ^{137}Cs in seawater by oceanic dispersion simulations. In the oceanic dispersion simulations, ^{137}Cs deposition by the atmospheric dispersion simulations were used as input from the atmosphere to oceans. The model descriptions, used source terms, validation data and simulation settings are described in Section 2. Section 3 shows the validation results of the atmospheric and oceanic dispersion simulations. This study concludes with Section 4.

2. Materials and method

2.1. Model description

2.1.1. Atmospheric-dispersion database system

In this study, we used WSPEEDI-DB (Terada et al., 2020b). This database system enables us to immediately obtain the prediction results by applying provided source terms (released radionuclides, release rate, and release period) to the database of dispersion-calculation results prepared in advance without specifying the source term. WSPEEDI-DB consists of an atmospheric dispersion model (GEARN) and a meteorological model, and the database is established from simulation results using both models.

GEARN is designed as an offline Lagrangian particle model and calculates the atmospheric dispersion of radionuclides by tracing the trajectories of numerous marker particles discharged from a single release point. The horizontal model coordinates (x and y directions) are the map coordinates, and the vertical coordinate is the terrain-following coordinate (z^*). By using meteorological variables, GEARN calculates the movement of each particle affected by both advection because of wind, and diffusion because of sub-grid scale turbulent eddy. In this study, the horizontal diffusion coefficient is based on Terada et al. (2013), and the vertical diffusion coefficient is calculated using a meteorological model included in WSPEEDI-DB. Some airborne radionuclides are deposited on the ground and sea surfaces by turbulence (dry deposition) and precipitation (wet deposition). In GEARN, the deposition of radionuclides because of turbulence is represented by 0.1 cm s^{-1} of dry deposition velocity and radioactivity of radionuclides (Terada and Chino, 2008). Furthermore, wet deposition processes are also included in GEARN. In studies by JAEA, several numerical schemes to calculate wet deposition processes were introduced in GEARN. The cloud microphysics including ice phase hydrometeors (in-cloud and below-cloud scavenging) for radioactive iodine gases (I_2 and CH_3I) and other particles (CsI, Cs, and Te) was introduced into GEARN by Katata et al. (2015). Furthermore, Katata et al. (2015) implemented fog-water deposition, cloud condensation nuclei activation, and subsequent wet scavenging, in GEARN. However, these numerical schemes are incorporated in GEARN in a form suited for local-scale high-resolution calculations, and their applicability for large-scale atmospheric dispersion simulations using coarse grid is unconfirmed. Therefore, in this study we used the simple deposition scheme (Terada and Chino, 2008), which was validated by large-scale simulations. In this study we assumed that the airborne ^{137}Cs exists as a particulate form, and wet deposition using the simple deposition scheme is calculated as in Eq. (1).

$$\frac{dq_n}{dt} = -\Lambda q_n \tag{1}$$

where q_n is the radioactivity of the n-th particle and Λ is the scavenging coefficient (s^{-1}), calculated as $\Lambda = 5 \times 10^{-5} \times (F_c I_c + F_n I_n)^{0.8}$. Variables I_c and I_n show the precipitation intensity (mm h^{-1}) of convective and non-convective rains for each grid cell, respectively, and are calculated using a meteorological model in WSPEEDI-DB. The values of F_c and F_n are 1 at grid cells below convective and non-convective cloud heights, respectively, and 0 at other grid cells.

In WSPEEDI-DB, the Advanced Research Weather Forecasting (WRF version 4.1) model is introduced as a meteorological model to simulate meteorological variables, which are used for calculating the transport of radionuclides in the atmosphere and their deposition. WRF is a non-hydrostatic, fully compressible model for mesoscale meteorological predictions developed at the National Center for Atmospheric Research (Skamarock et al., 2008) and can calculate meteorological variables such as wind velocity, diffusion coefficients, and precipitation based on

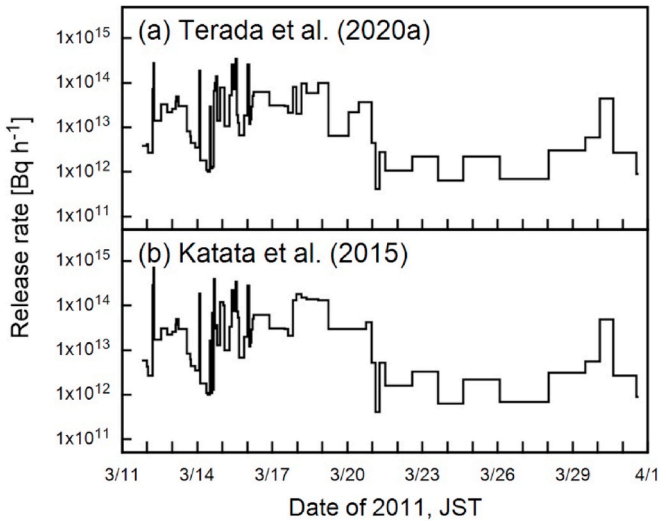

Fig. 1. Time series of the atmospheric release rates (Bq h^{-1}) of ^{137}Cs because of the FDNPS accident, which are used in this study, referenced from (a) Terada et al. (2020a) and (b) Katata et al. (2015).

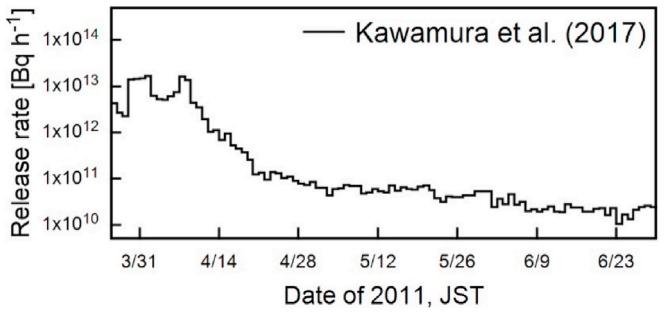

Fig. 2. Time series of the oceanic release rate (Bq h^{-1}) of ^{137}Cs because of the FDNPS accident, which is used in this study, referenced from Kawamura et al. (2017). The release rate before March 25, 2011 and after July 1, 2011 were set to as 0 Bq h^{-1}.

various physical options to parameterize turbulence, radiation, grid-resolved or grid-unresolved cloud processes, and land surface processes.

2.1.2. Oceanic dispersion model

To validate the reproducibility of ^{137}Cs concentrations in sea surface water, we also conducted an oceanic dispersion simulation using SEA-GEARN-FDM. SEA-GEARN-FDM is designed as the finite difference oceanic dispersion model developed by JAEA (Kawamura et al.,2014, 2017). SEA-GEARN-FDM has a function to simulate concentrations of radionuclides in seawater by both advection because of oceanic current and diffusion because of sub-grid scale turbulent eddy. When simulating the oceanic dispersion of radionuclides, SEA-GEARN-FDM considers the direct release of radionuclides from a nuclear facility into the ocean and deposition of radionuclides from the atmosphere as additional radionuclide input. The horizontal diffusion coefficient in SEA-GEARN-FDM is calculated based on the formula by Smagorinsky (1963). The vertical diffusion coefficients are 1.0×10^{-3} m^2 s^{-1} and 1.0×10^{-5} m^2 s^{-1} above and below the mixed-layer depth, respectively (Kawamura et al., 2017). In this study, the oceanographic data calculated using the ocean data assimilation system, MOVE/MRI.COM developed at the Meteorological Research Institute of Japan Meteorological Agency (Usui et al., 2006), were used as input data of the oceanic dispersion simulation by SEA-GEARN-FDM. The details of the oceanographic data used in this study are shown in Kawamura et al. (2017).

2.2. Source terms

In this study, we validated the source terms of ^{137}Cs released in the atmosphere because of the FDNPS accident estimated by Terada et al. (2020a) by applying it as input data for large-scale atmospheric dispersion simulations. For this validation, we also conducted the large-scale atmospheric dispersion simulation using the source term by Katata et al. (2015). Fig. 1 shows the time series of the atmospheric release rates used in this study. Based on measured sea surface ^{137}Cs concentrations near the northern and southern discharge channels of FDNPS, Kawamura et al. (2011) and Kawamura et al. (2017) estimated the direct release rate of ^{137}Cs into the ocean. In the oceanic dispersion simulation, we used the source term by Kawamura et al. (2017) and assumed that the direct release of ^{137}Cs into the ocean continued from March 26 to June 30, 2011 (Fig. 2).

2.3. Measurement data for validation

To validate large-scale atmospheric dispersion simulations using the source term by Terada et al. (2020a), we used concentrations of airborne ^{137}Cs sampled from the IMS stations. In this study, we extracted 24 stations, where the airborne ^{137}Cs attributed to the FDNPS accident was detected in March 2011, from all IMS stations in the calculated domain. These stations were categorized as Pacific and Other by their locations (Table 1 and Fig. 3). In this study, we defined the Pacific as the extracted stations in the Pacific Ocean, Pacific Rim and North America, except for the polar region. Concentrations of ^{137}Cs in the sea surface water simulated in this study were compared with measurement data reported by Aoyama et al. (2013) who compiled ^{137}Cs concentrations in seawater in the North Pacific after the FDNPS accident. Fig. 4 shows the measurement points of ^{137}Cs concentrations used in validation.

2.4. Simulation settings

Tables 2 and 3 summarize the simulation settings of WRF and GEARN, respectively. In this study, we conducted four atmospheric dispersion simulations using WRF and GEARN. In these simulations, either the source term by Terada et al. (2020a) or Katata et al. (2015) was used. The source term used in each simulation is shown as the label of T20 (Terada et al., 2020a) and K15 (Katata et al., 2015) in the name of the simulations. Simulations, ATM-P_T20 and ATM-P_K15, covers the Northern Hemisphere, and the others, ATM-M_T20 and ATM-M_K15, mainly covers the North Pacific (Table 3). In these simulations, different map projections were used based on their calculated domains (Figs. 3 and 4). The uncertainty of atmospheric dispersion of ^{137}Cs originates from the different simulation domains. The consistency between the results of the simulations using the source term by Terada et al. (2020a) are discussed in Appendix A.

When comparing simulated air concentrations of ^{137}Cs with the measurements at the IMS stations, the results of ATM-P_T20 and ATM-P_K15 were mainly used. Furthermore, we validated the ^{137}Cs deposited at the sea surface in the North Pacific. However, it was impossible to directly validate the ^{137}Cs deposition obtained from atmospheric dispersion simulation because of no available measurement data of ^{137}Cs deposition over oceans. Therefore, as in Kawamura et al. (2017), we conducted oceanic dispersion simulations, OCN_T20 and OCN_K15, using SEA-GEARN-FDM (Table 4). In these simulations, we used the deposition flux of ^{137}Cs simulated by WSPEEDI-DB as an influx from the atmosphere to ocean surfaces and compared concentrations of ^{137}Cs in the sea surface water simulated by SEA-GEARN-FDM with the measurement data. Although this methodology proposed by Kawamura et al. (2017) is not a direct validation of ^{137}Cs deposition, we indirectly confirmed the validity of the ^{137}Cs deposition over oceans from the atmospheric dispersion simulations by verifying the ^{137}Cs concentration in the sea surface water. Fig. 4 and Table 4 show the calculation domain and the simulation settings for OCN_T20 and OCN_K15, respectively.

Table 1
Sites of the IMS stations used in this study. The Pacific region was defined as the IMS stations in the Pacific Ocean, Pacific Rim and North America, except for the polar region of North America.

Region	ID	Station code	Station name	Country	Latitude	Longitude
Pacific						
	1	CAP14	Vancouver, B.C.	Canada	48.65°N	123.45°W
	2	CAP16	Yellowknife, N.W.T.	Canada	62.48°N	114.47°W
	3	CAP17	St. John's N.L.	Canada	47.59°N	52.74°W
	4	JPP37	Okinawa	Japan	26.5°N	127.9°E
	5	JPP38	Takasaki, Gunma	Japan	36.3°N	139.08°E
	6	RUP60	Petropavlovsk-Kamchatskiy	Russia	53.05°N	158.78°E
	7	USP70	Sacramento, CA	USA	38.67°N	121.36°W
	8	USP71	Sand Point, AK	USA	55.34°N	160.49°W
	9	USP72	Melbourne, FL	USA	28.1°N	80.65°W
	10	USP74	Ashland, KS	USA	37.17°N	99.77°W
	11	USP75	Charlottesville, VA	USA	38°N	78.4°W
	12	USP76	Salchaket, AK	USA	64.67°N	147.1°W
	13	USP77	Wake Island	USA	19.29°N	166.61°E
	14	USP78	Midway Islands	USA	28.22°N	177.37°W
	15	USP79	Oahu Island, HI	USA	21.52°N	157.99°W
Other						
	16	DEP33	Schauinsland, Freiburg	Germany	47.92°N	7.91°E
	17	MNP45	Ulaanbaatar	Mongolia	47.89°N	106.33°E
	18	PTP53	Ponta Delgada	Portugal	37.74°N	25.7°W
	19	RUP54	Kirov	Russia	58.59°N	49.41°E
	20	RUP59	Zalesovo	Russia	53.94°N	84.79°E
	21	SEP63	Stockholm	Sweden	59.41°N	17.95°E
	22	CAP15	Resolute, NU	Canada	74.71°N	94.97°W
	23	ISP34	Reykjavik	Iceland	64.09°N	21.84°W
	24	NOP49	Spitsbergen	Norway	78.23°N	15.39°E

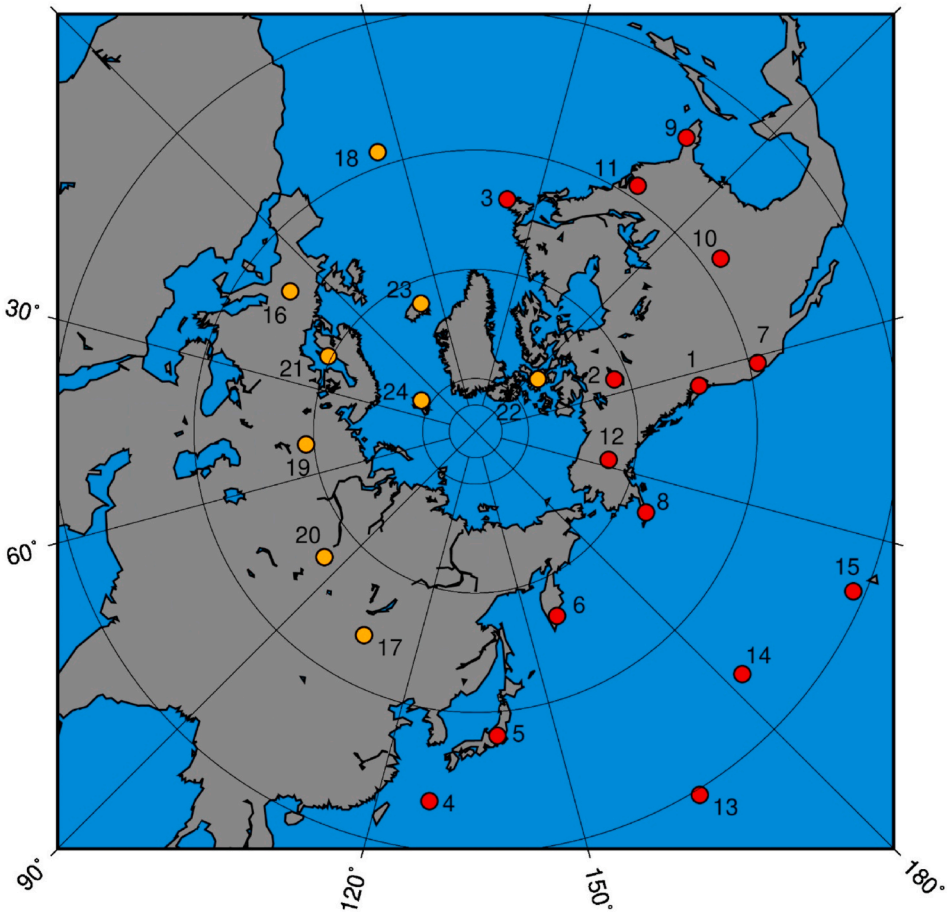

Fig. 3. Calculation domain for the atmospheric dispersion simulations of ATM-P_T20 and ATM-P_K15. Table 3 shows the details of both simulations. The dots show the locations of the IMS stations at which the air concentrations of ^{137}Cs used in this study are measured. The colored dots indicate the IMS stations categorized as Pacific (red) and Other (orange) regions (Table 1). The numbers from 1 to 24 in the figure correspond to the ID of the IMS stations in Table 1. The Pacific region was defined as the IMS stations in the Pacific Ocean, Pacific Rim and North America, except for the polar region. (For interpretation of the references to color in this figure legend, the reader is referred to the Web version of this article.)

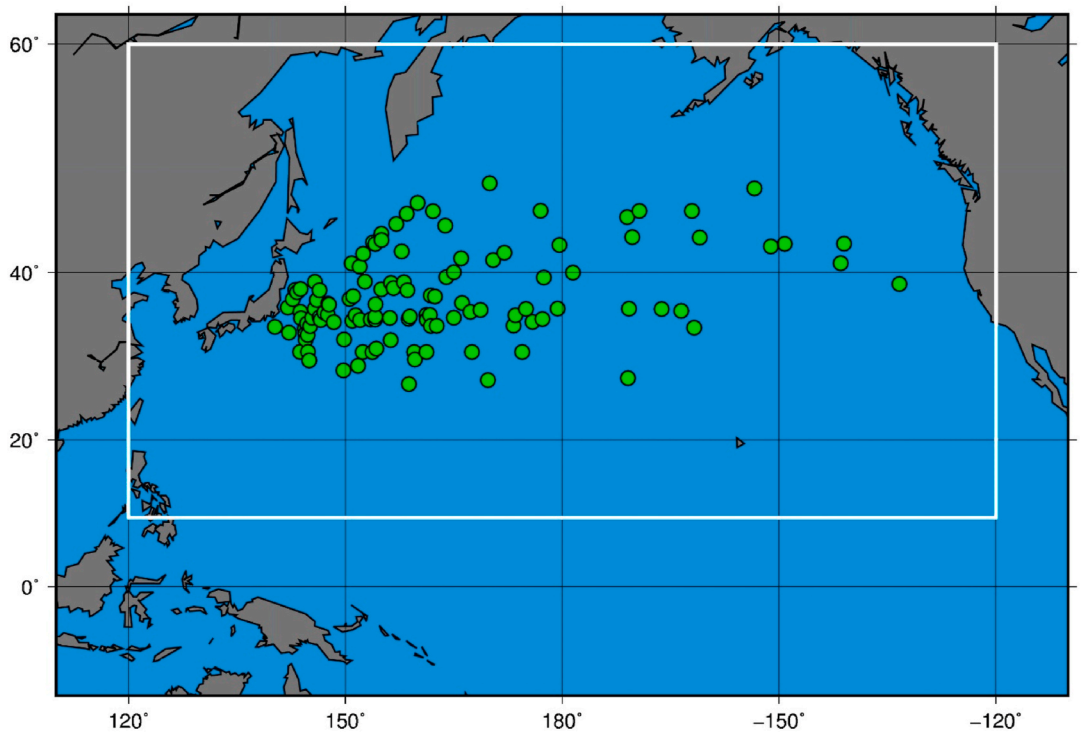

Fig. 4. Calculation domains for the atmospheric (ATM-M_T20 and ATM-M_K15) and oceanic (OCN_T20 and OCN_K15) dispersion simulations. Tables 3 and 4 show the details of the atmospheric and oceanic dispersion simulations, respectively. The white box indicate the domain of the oceanic dispersion simulation. The green dots show the measurement points of ^{137}Cs concentration in seawater, reported by Aoyama et al. (2013). (For interpretation of the references to color in this figure legend, the reader is referred to the Web version of this article.)

Table 2
Simulation settings of WRF for atmospheric dispersion simulations. The result of the simulation using polar stereographic was used in ATM-P_T20 and ATM-P_K15, and that using Mercator was used in ATM_M-T20 and ATM-M-K15.

Term	Setting
Model	WRF version 4.1
Period	11 March to April 1, 2011
Horizontal grid number	310 × 310 540 × 340
Horizontal resolution	54 km × 54 km
Map projection	Polar stereographic Mercator
Vertical levels	31 eta levels from surface to 100 hPa
Boundary condition	Grid Point Value of Global Spectral Model by Japan Meteorological Agency
Physical scheme	
Planetary boundary layer	Mellor-Yamada-Nakanishi-Niino Level 2.5 (Nakanishi and Niino, 2004)
Cloud microphysics	Morrison double-moment scheme (Morrison et al., 2005)
Cumulus	Betts-Miller-Janjic scheme (Betts and Miller 1993)
Shortwave radiation	Rapid Radiative Transfer Model (Mlawer et al., 1997)
Longwave radiation	Dudhia scheme (Dudhia, 1989)
Land surface	5-layer thermal diffusion scheme

Table 3
Simulation settings of GEARN for atmospheric dispersion simulations. Figs. 3 and 4 show the simulation domains of ATM-P_T20 and ATM-P_K15, and ATM-M_T20 and ATM-M_K15, respectively.

Setting				
Term	Simulation			
	ATM-P_T20	ATM-M_T20	ATM-P_K15	ATM-M_K15
Period	11 March to April 1, 2011			
Horizontal grid number	307 × 307	537 × 337	307 × 307	537 × 337
Horizontal resolution	54 km × 54 km			
Map projection	Polar stereographic	Mercator	Polar stereographic	Mercator
Vertical levels[a]	29 levels from surface to 10,000 m			
Released particle number	1,000,000/ hour	800,000/ hour	1,000,000/ hour	800,000/ hour
Source term	Terada et al. (2020a)		Katata et al. (2015)	

[a] Vertical levels of the model's lower layers are 10, 42.5, 99.9, 182.4, 289.2, 422.2, 579.5, 761.9, and 969.2 m.

The calculation domain of ATM-P_T20 and ATM-P_K15 (Fig. 3) did not completely cover that of OCN_T20 and OCN_K15 (Fig. 4). Therefore, we used the deposition flux of ^{137}Cs from ATM-M_T20 and ATM-M_K15 (Table 3) as input data of OCN_T20 and OCN_K15, respectively. Terada et al. (2012) and Kawamura et al. (2017) reported that the surface deposition of ^{137}Cs in eastern Japan was mainly formed in March 2011. Furthermore, aerially released ^{137}Cs was mostly released in March 2011 (Terada et al., 2020a). Therefore, we used the deposition flux of ^{137}Cs from the release in March 2011 for the input data. The calculation period of OCN_T20 and OCN_K15 was from March 11, 2011 to April 1, 2012, which was determined based on the measurement periods reported by Aoyama et al. (2013).

3. Results and discussion

3.1. Validation of precipitations

Airborne ^{137}Cs exist mainly in particulate form and are removed from the atmosphere via dry and wet deposition processes. Wet deposition from rainfall can effectively remove ^{137}Cs from the atmosphere. Therefore, the reproducibility of precipitation used in simulations is critical for the long-range transport of airborne ^{137}Cs. Fig. 5 shows the

Table 4
Simulation setting of SEA-GEARN-FDM for the oceanic dispersion simulations.

Setting		
Term	Simulation	
	OCN_T20	OCN_K15
Period	March 11, 2011 to April 1, 2012	
Domain	10.1°N–60.1°N, 120.1°E−120.0°W	
Horizontal resolution	0.10 ° × 0.10 °	
Vertical levels	54 levels from surface to 6300 m	
Initial condition of ^{137}Cs concentration	0 Bq m^{-3}	
Boundary condition of ^{137}Cs between the atmosphere and oceans	^{137}Cs deposition flux by ATM-M_T20	^{137}Cs deposition flux by ATM-M_K15
Lateral boundary condition of ^{137}Cs	No input of ^{137}Cs from out of domain	
Source term	Kawamura et al. (2017)	
Diffusion scheme		
Horizontal diffusion	Smagorinsky (1963)	
Vertical diffusion coefficient (above mixed-layer depth)	1.0 × 10^{-3} m^2 s^{-1}	
Vertical diffusion coefficient (below mixed-layer depth)	1.0 × 10^{-5} m^2 s^{-1}	

precipitation (mm) from the simulation result used in ATM-M_T20 and ATM-M_K15, with the reanalysis product of GsMAP (Kubota et al., 2020). The precipitations shown in Fig. 5 accumulated from March 12–31, 2011, because ^{137}Cs deposition from the FDNPS accident mostly occurred in this period (Kawamura et al., 2017). In March 2011, a tropospheric jet transported the plume including a large amount of ^{137}Cs from FDNPS (green squares in Fig. 5) to the eastern area of the Aleutian Islands (Stohl et al., 2012). Over this pathway from FDNPS to the northeast, the horizontal distribution of the simulated precipitation correlated well with that of GsMAP except for the areas of no data in Fig. 5. Therefore, from FDNPS to the northeast, we can perform the dispersion analysis for the simulation result based on the good reproducibility of precipitation.

However, compared to the precipitation in other areas of the North Pacific, the simulated precipitation was underestimated. In the subtropics (10°N–20°N), the accumulated precipitation in the simulation was smaller than that of the measurement (Fig. 5). Particularly, the underestimation was remarkable in the western part of the subtropic. The subtropics are near the boundary of the simulation domain. Therefore, the underestimation could be because of an inflow condition of water vapor in the simulation. While the precipitation was smaller in the subtropics, this area is out of the major pathway of hemispheric-scale atmospheric transport of ^{137}Cs aerially released from FDNPS (Stohl et al., 2012; Winiarek et al., 2012; Mészáros et al., 2016; Sarkar et al., 2017). Since the wind fields used in the atmospheric dispersion simulations were well simulated by WRF (not shown), the underestimated precipitation in the subtropics would not critically affect air concentrations and depositions of ^{137}Cs in the simulation.

The precipitation from 20°N to 45°N in the North Pacific was regionally underestimated, as shown by X and Y areas in Fig. 5. Fig. 6 shows the time series of daily precipitations averaged over the X and Y areas in March 2011. Although the simulation reasonably captured the rainfall dates in the X area, overall simulated precipitation intensity was smaller than the measurement (Fig. 6a). Particularly, the precipitation measured on March 16 was ~48 mm and was the largest intensity in March 2011, corresponding to half of the total precipitation in this month, but the WRF did not well simulate this precipitation. Therefore, the underestimation of precipitation in the X area in Fig. 5 mainly resulted from less precipitation on March 16. Furthermore, the simulated precipitation in the middle latitude north of 30°N in the eastern North Pacific, shown as the Y area in Fig. 5, was also smaller than the measurement (Fig. 6b). Here, remarkable rainfall was measured on March 12, 15–19, 25–27, and 31; however, these measurements were mostly underestimated in the WRF simulation. Studies have revealed that several plumes of ^{137}Cs from FDNPS passed over the above-mentioned areas in March 2011. Therefore, to analyze and discuss the results of the dispersion simulations, WRF precipitation underestimation and reasonable precipitation in the western North Pacific should be considered.

3.2. Comparison of air concentrations

To confirm the availability of the source term by Terada et al. (2020a) to reproduce the hemispheric-scale dispersion of ^{137}Cs, first, we statistically compared the air concentrations of ^{137}Cs calculated by WSPEEDI-DB with the measurement at IMS stations. Fig. 7 shows scatter plots of the daily-mean air concentration of ^{137}Cs comparing the hemispheric-scale atmospheric dispersion simulations (ATM-P_T20 and ATM-P_K15) with the measurement. The zones between the dashed lines describe the area satisfying with a factor of 10 (*FA10*). *Bias* is an indicator of overestimation or underestimation, and in this study was calculated using Eq. (2).

$$Bias = \frac{1}{n}\sum \log_{10}\left(\frac{C_S}{C_M}\right) \quad (2)$$

where C_S and C_M are simulation and measurement values of daily-mean ground-level air concentrations of ^{137}Cs at monitoring stations, respectively, and n is the total number of pairs for the values compared. The positive (negative) value of *Bias* shows overestimation (underestimation) of the simulation, and the value closer to 0 indicates higher agreement between the simulation and measurement. From the statistical analysis for the result of ATM-P_T20, a value of *FA10* for the total region was calculated as 0.74 (Fig. 7a). This value was higher than that from the result of ATM-P_K15 (*FA10* = 0.71) (Fig. 7b). The *Bias* value from the result of ATM-P_T20 was 0.20, indicating that ^{137}Cs concentrations by ATM-P_T20 were slightly overestimated. However, this value was lower than the *Bias* value of 0.37 from the result of ATM-P_K15. The result of these comparisons shows the better reproducibility of air concentrations of ^{137}Cs by ATM-P_T20 than ATM-P_K15. For the Pacific region, the *FA10* and *Bias* values from the result of ATM-P_T20 were 0.72 and 0.28, respectively (Fig. 7c). These values were the same level as the total region (Fig. 7a) because the compared data were mostly included in the Pacific region. As well as the total region, these values show the better reproducibility of air concentrations of ^{137}Cs in the Pacific region by ATM-P_T20 than ATM-P_K15 because of 0.68 and 0.45 of the *FA10* and *Bias* values, respectively, for ATM-P_K15 (Fig. 7d). For other, including Europe, Asia, and Arctic region, the *FA10* and *Bias* values from the result of ATM-P_T20 were 0.81 and −0.09, respectively (Fig. 7e). These values of *FA10* and *Bias* were the same level as ATM-P_K15 (*FA10* = 0.82, *Bias* = 0.09) (Fig. 7f). For both simulations, when comparing with the Pacific, the *FA10* and *Bias* values for other were higher and smaller than those of Pacific, respectively. While the compared number of data was relatively small, this result shows that the high reproducibility of air concentrations of ^{137}Cs at the IMS stations in Europe, Asia, and Arctic regions from the results of ATM-P_T20 and ATM-P_K15.

Next, we compared the time series of air concentrations of ^{137}Cs. Fig. 8 shows the time series of daily-mean ground-level air concentrations (Bq m^{-3}) of ^{137}Cs at the IMS stations. In this comparison, we used the simulated air concentrations at the bottom layer with the 20 m thickness. Totally, the time series of the air concentrations by ATM-P_T20 showed the similar variation of that by ATM-P_K15. The both simulations well captured the day when the ^{137}Cs concentration started exceeding the detection limit (1.0 × 10^{-6} Bq m^{-3}) at each IMS station. The detection time lag between the simulation and measurement results was within one day except for JPP37 (5 days of lag) and MNP45 (2 days of lag), showing that the hemispheric-scale atmospheric dispersion of ^{137}Cs aerially released from FDNPS was well reproduced by ATM-P_T20

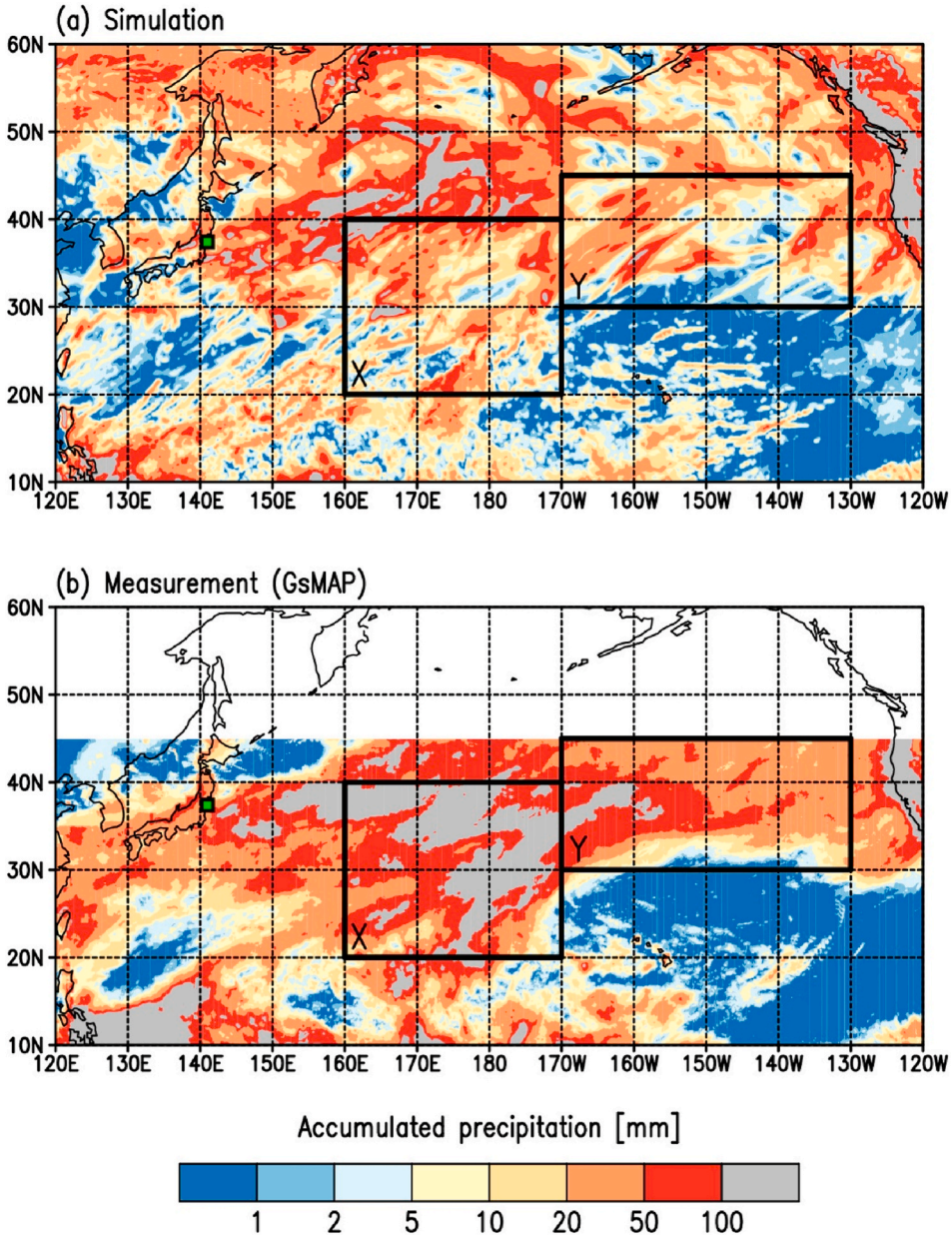

Fig. 5. Accumulated precipitation (mm) from March 12 to 31, 2011, derived from (a) the WRF simulation and (b) reanalysis product based on measurements. In this study, we used GsMAP_Gauge_RNL as the reanalysis product (Kubota et al., 2020). Boxes X and Y show the areas in which the underestimation of the precipitation against the measurement was outstanding. The green square in each figure the location of FDNPS. Blue (put in the most left) and gray (put in the most right) of the color bar means the accumulated precipitation from 0 to 1 mm and more than 100 mm, respectively. (For interpretation of the references to color in this figure legend, the reader is referred to the Web version of this article.)

and ATM-P_K15. Peak concentrations of ^{137}Cs were observed at several stations, and the timing of the peaks was reasonably simulated by ATM-P_T20 and ATM-P_K15. For the Pacific region, the peak concentration for CAP14 observed on March 24 (Fig. 8a), consistent with the measurement results. Similarly, for JPP38, remarkable peaks were simulated on March 15, 20, and 30, well corresponding to the measurement at IMS stations (Fig. 8e). As well as JPP38, multiple peaks of the air concentration of ^{137}Cs for USP78 using WSPEEDI-DB were consistent with the measurements (Fig. 8n). For other, the ATM-P_T20 and ATM-P_K15 simulations well captured an increase or decrease in air concentrations of ^{137}Cs, even though the stations are far from FDNPS. The results show that the time series of air concentrations of ^{137}Cs in the hemispheric-scale atmospheric dispersion simulations using WSPEEDI-DB with the source term by Terada et al. (2020a) or Katata et al. (2015) were reasonable, indicating that the spatial distribution of air concentrations of ^{137}Cs in this study would be reproduced well.

For ATM-P_T20 and ATM-P_K15, high concentrations of airborne ^{137}Cs, which were undetected by the measurement at the IMS stations, were simulated at JPP37 and USP77 of the IMS stations for March 20–21 (Fig. 8d) and March 19–21 (Fig. 8m), respectively. Fig. 9 shows the temporal development of horizontal distribution of daily-mean ground-level air concentrations of ^{137}Cs from ATM-P_T20. Because the spatio-temporal distribution of the air concentrations of ^{137}Cs by ATM-P_K15 was mostly same as that by ATM-P_T20, the distribution from the result of ATM-P_K15 is not shown in this paper. The edge of the ^{137}Cs plume was passed over sites JPP37 and USP77 from March 19 to 21, and large gradients of the air concentrations occurred along the edge. Therefore, the high concentrations for JPP37 and USP77 could be because of the horizontal resolution of the simulation. Furthermore, the simulation overestimated air concentrations of ^{137}Cs for CAP14, USP70, USP74, USP77 and USP79 of the IMS stations (Fig. 8a, g, 8j, 8m, and 8°) in late March. Except for USP74 in the Midwestern United State, these stations are distributed in the North Pacific and along the coastal area (Table 1), indicating that the uncertainty of the long-range transport of ^{137}Cs that have passed over the North Pacific could be large in ATM-P_T20 (and also ATM-P_K15). Further discussion regarding this uncertainty is described in Section 3.4.

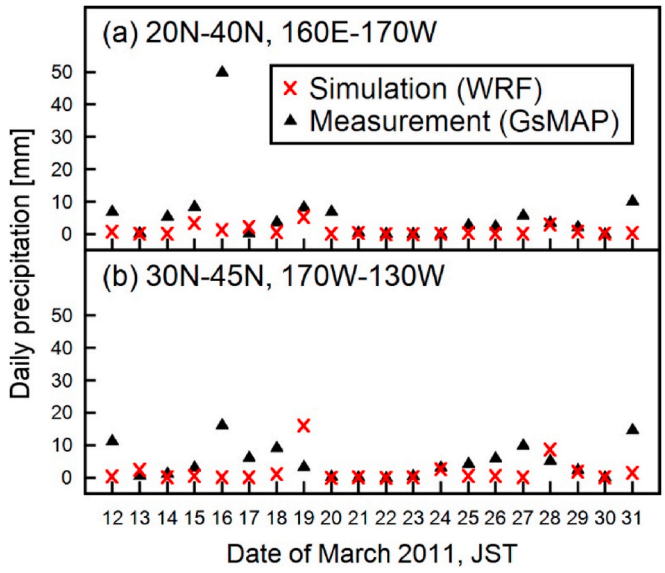

Fig. 6. Time series of daily precipitation (mm) derived from the WRF simulation and reanalysis product (GsMAP_Gauge_RNL, Kubota et al., 2020) based on measurements. The precipitation in Fig. 6a and b is averaged over 20°N–40°N and 160°E–170°W (the area of X in Figs. 5), and 30°N–45°N and 170°W–230°W (the area of Y in Fig. 5), respectively.

3.3. Accuracy of ^{137}Cs deposition

In Section 3.2, we compared the air concentrations of ^{137}Cs simulated by WSPEEDI-DB using the measurements at the IMS stations and showed the high performance of the hemispheric-scale atmospheric dispersion simulation using the source term by Terada et al. (2020a). We also showed the uncertainty of the long-range transport of airborne ^{137}Cs in the North Pacific. However, airborne ^{137}Cs are readily removed from the atmosphere via wet deposition process because of their particulate form, and thus it is also critical to validate the reproducibility of ^{137}Cs deposition. Therefore, we discuss the accuracy of ^{137}Cs deposition by the hemispheric-scale atmospheric dispersion simulations. The total deposition amount of ^{137}Cs on land was directly compared with the measurement. By using ^{137}Cs concentrations in the sea surface water from OCN_T20 and OCN_K15 and the methodology described in Section 2.4, the deposition of ^{137}Cs over the North Pacific was indirectly validated.

3.3.1. Deposition on land

Fig. 10 shows the horizontal distribution of the deposition density (Bq m^{-2}) of ^{137}Cs on April 1, 2011, obtained from the result of ATM-M_T20. The deposition amount of ^{137}Cs in the comparable area (the land area surrounded by white lines in Fig. 10) was 1.9 PBq. This deposition amount exhibits the good reproducibility of terrestrial deposition amount of ^{137}Cs in comparison with the airborne monitoring, 2.4 PBq by MEXT (MEXT, 2012). Similarly, the deposition amount by ATM-M_K15 was calculated as 2.3 PBq. This value is closer to the airborne monitoring than the deposition amount by ATM-M_T20. This is

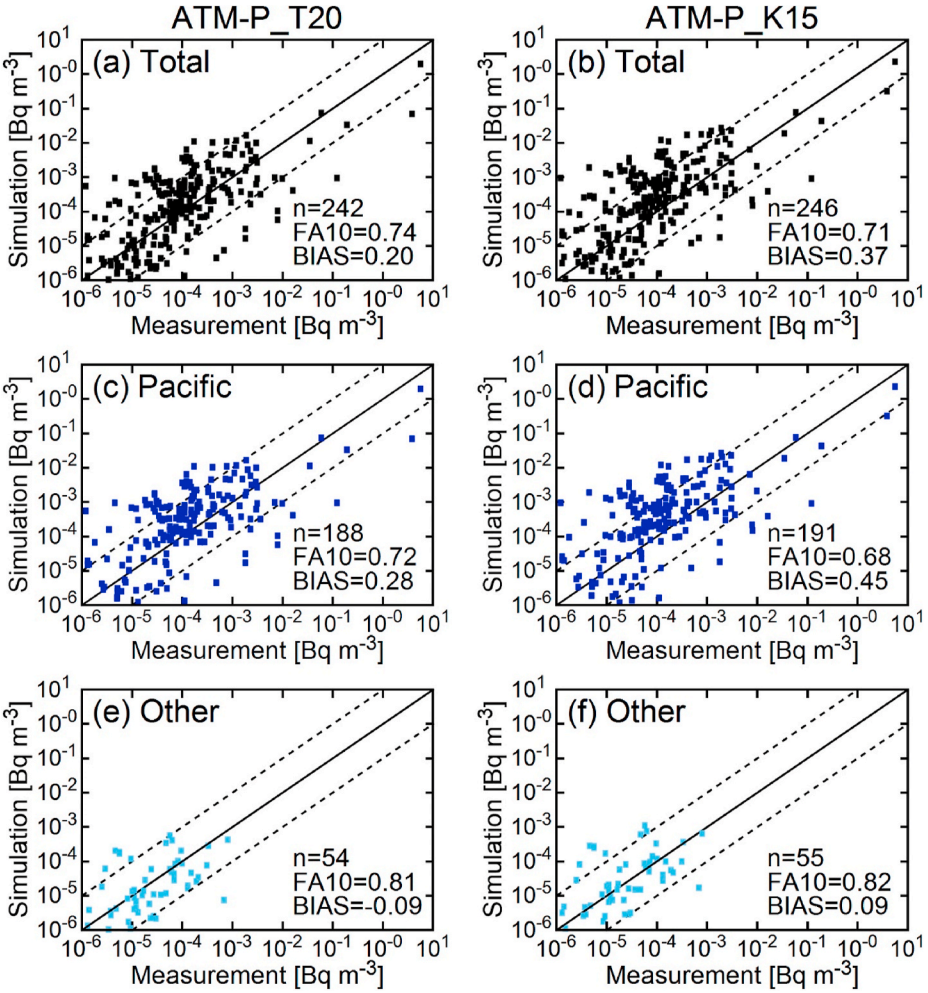

Fig. 7. Scatter plots of daily-mean ground-level air concentrations (Bq m^{-3}) of ^{137}Cs obtained from simulations (ATM-P_T20 and ATM-P_K15) and the measurement at the IMS stations. The plots in the left and right are the results from A TM-P_T20 and ATM-P_K15, respectively. Top, middle, and bottom figures show (a, b) total, (c, d) Pacific, and (e, f) other, respectively. The zones between the dashed lines describe the area satisfying with a factor of 10 (*FA10*). In this comparison, we used the simulated air concentrations at the bottom layer with the 20 m thickness.

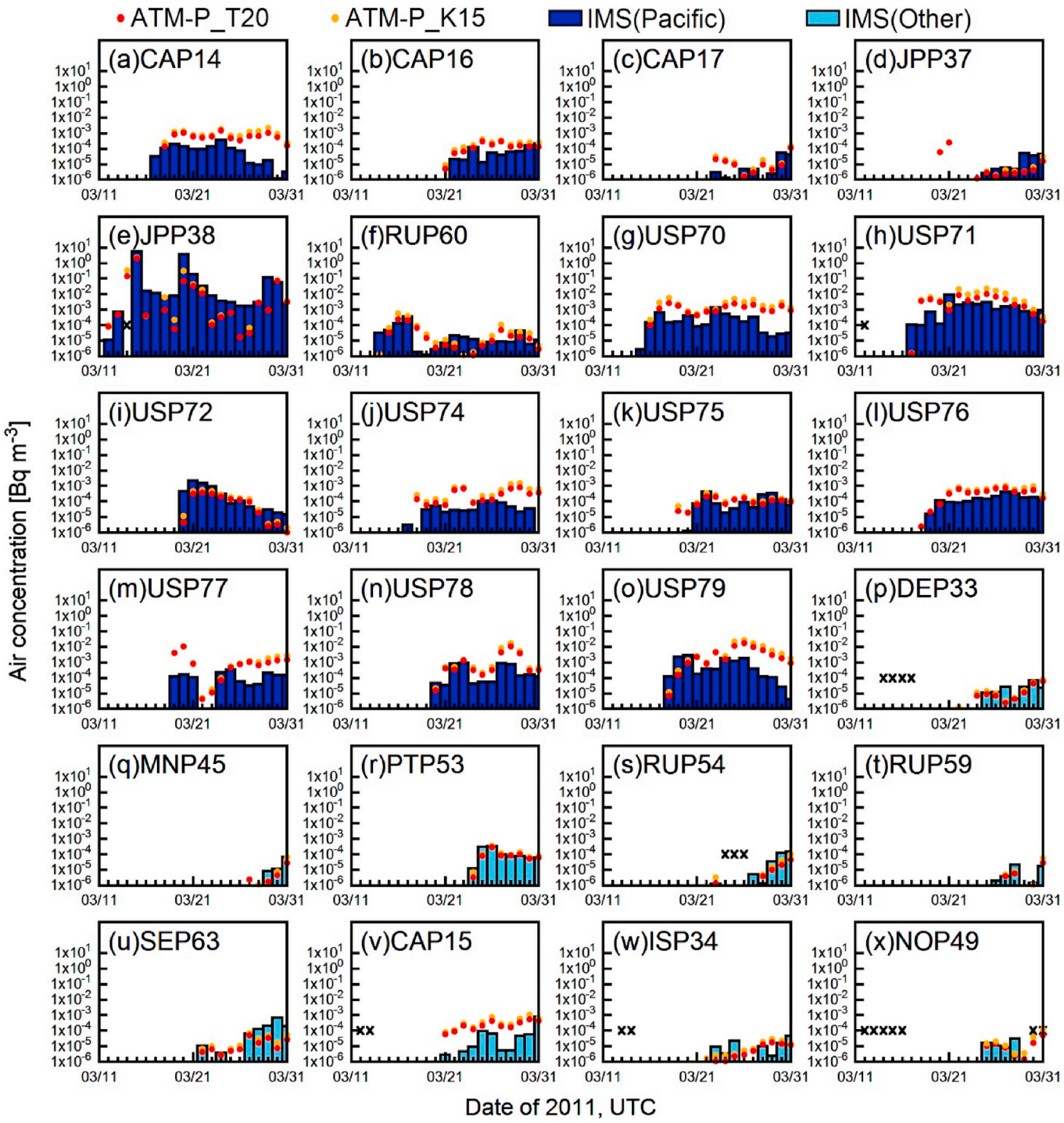

Fig. 8. Time series of daily-mean ground-level air concentrations (Bq m^{-3}) of ^{137}Cs obtained from ATM-P_T20, ATM-P_K15, and the measurements at the IMS stations. Table 1 summarized the comparison sites. Missing values of the measurement are shown as the x-mark. The blue and light blue bars correspond to Pacific and other regions, respectively (Table 1). In this comparison, we used the simulated air concentrations at the bottom layer with the 20 m thickness. (For interpretation of the references to color in this figure legend, the reader is referred to the Web version of this article.)

because the release amount of ^{137}Cs using ATM-M_K15 was totally larger than that using ATM-M_T20 (Fig. 1). In the atmospheric dispersion simulations of this study, the remarkable deposition occurred by March 15. Therefore, the reproducibility of the deposition amount over the land area by ATM-M_T20 may be improved by increasing the release amount of ^{137}Cs from March 11 to 15. However, when achieving the improvement, the influence on the reproducibility of air concentrations and deposition over oceans should be considered.

Terada et al. (2020a) estimated that the amount of ^{137}Cs deposited at the ground surface near FDNPS on April 1, 2011 was 2.1 PBq by the local-scale atmospheric simulation using atmospheric release from March 11 to April 1, 2011. The difference of the deposition amount between ATM-M_T20 and Terada et al. (2020a) was 0.2 PBq. This study focused on the large-scale atmospheric dispersion of ^{137}Cs due to the FDNPS accident, and the spatial resolution used in this study was coarser than that in Terada et al. (2020a). Therefore, when calculating the deposition amount from the simulation result of this study, the land targeted by the airborne monitoring should not be precisely captured.

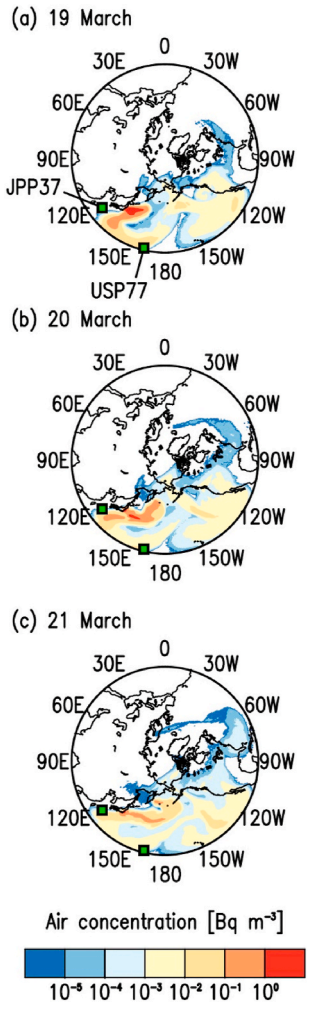

Fig. 9. The horizontal distribution of daily-mean ground-level air concentrations (Bq m^{-3}) of ^{137}Cs between March 19 and 21 obtained from ATM-P_T20.^{137}Cs concentrations less than 1.0×10^{-6} Bq m^{-3} are not shown in the figures. The green dots show the locations of JPP37 and USP77. In this comparison, we used the simulated air concentrations at the bottom layer with the 20 m thickness. Blue (put in the most left) and red (put in the most right) of the color bar means the air concentration from 1.0×10^{-6} to 1.0×10^{-5} Bq m^{-3} and more than 1 Bq m^{-3}, respectively. The air concentration lower than 1.0×10^{-6} Bq m^{-3} is not colored in the figure. (For interpretation of the references to color in this figure legend, the reader is referred to the Web version of this article.)

However, the difference of 0.2 PBq was only 2 % of total amount of aerially released ^{137}Cs in March 2011. This accordance evidences the good consistency between the results of local and large-scale atmospheric dispersion simulations using the source term by Terada et al. (2020a).

3.3.2. *Deposition over oceans*

In this study, the global fallout of ^{137}Cs attributed to atomic weapons tests in the 20th century was not considered in the simulation. Therefore, when analyzing ^{137}Cs concentrations in the sea surface water, we added 1 Bq m^{-3}, estimated as the background level of ^{137}Cs concentrations in the sea surface water by Aoyama et al. (2008), to those of simulation results. Fig. 11 shows a scatter plot of ^{137}Cs concentrations (Bq m^{-3}) in the sea surface water between the oceanic dispersion simulations (OCN_T20 and OCN_K15) and the measurement data reported by Aoyama et al. (2013). The simulations well reproduced the measured concentrations of ^{137}Cs in the sea surface water, with high scores of *FA10* (0.96 and 0.97 from the results of OCN_T20 and OCN_K15, respectively). These values support that the deposition density of ^{137}Cs simulated by WSPEEDI-DB were statistically reasonable over the North Pacific. However, when adopting Eq. (2) to concentrations of ^{137}Cs in sea surface water instead of air concentrations of ^{137}Cs, the *Bias* values from the results of OCN_T20 and OCN_K15 were calculated as −0.20 and −0.11, respectively. This shows that the ^{137}Cs concentrations in the sea surface water from the simulations in this study were slightly underestimated (Fig. 11). The underestimation of ^{137}Cs concentrations in the sea surface water was also seen in Kawamura et a. (2017), which was significant in the eastern North Pacific with the underestimation of air concentrations of ^{137}Cs over the Pacific region, unlike the overestimation of those in this study. Kawamura et al. (2017) reported that the underestimation of ^{137}Cs concentrations in the sea surface water could result from less atmospheric transport of ^{137}Cs from FDNPS to the oceans.

Before discussing the atmospheric transport of ^{137}Cs, we investigated the geographical distribution of ^{137}Cs concentrations in the sea surface water simulated in this study. Fig. 12 shows a box plot of ^{137}Cs concentrations in the sea surface water from March 2011 to April 2012 every 10° in longitude, obtained from the results of OCN_T20 and OCN_K15. When focusing on the North Pacific from 140°E to 150°E, the 25th–75th percentiles (boxes in Fig. 12) of ^{137}Cs concentrations in the sea surface water by the simulations were included in those of the measurement, and the median values (horizontal bars in boxes in Fig. 12) of those by SEA-GEARN-FDM acceptably agreed to the measurement. Because WRF and SEA-GEARN-FDM reasonably simulated the precipitation and ^{137}Cs concentrations in the sea surface water in this longitude zone, respectively, the total deposition amount of ^{137}Cs by OCN_T20 and OCN_K15 would be reasonable from 140°E to 150°E. Similarly, the ^{137}Cs concentrations in the sea surface water from 160°E to 170°E were acceptably reproduced by SEA-GEARN-FDM, with good agreement in both the percentiles and median values. The results indicate that the total deposition amount of ^{137}Cs by OCN_T20 and OCN_K15 would be reasonable from 160°E to 170°E. From 150°E−160°E, the median values for ^{137}Cs concentrations in the sea surface water by OCN_T20, OCN_K15 and Aoyama et al. (2013) were 5.6 Bq m^{-3}, 8.2 Bq m^{-3}, and 13.3 Bq m^{-3}, respectively, showingh the underestimate of the ^{137}Cs concentrations by SEA-GEARN-FDM. In the simulations, the atmospheric deposition of ^{137}Cs after April 2011 was not considered. This simulation setting could influence on the underestimation. Furthermore, the underestimation of ^{137}Cs concentrations in the sea surface water from 170°E to 230°E was relatively large. However, note that these statistical results have a large uncertainty because the number of used comparison data was small, especially from 200°E to 230°E. Because ^{137}Cs directly released in oceans was not transported to the eastern North Pacific within one year after the FDNPS accident (Kawamura et al., 2017), overall underestimation from 170°E to 230°E could be because of the less amount of ^{137}Cs transported from the atmosphere to the oceans. This result indicates that WSPEEDI-DB would underestimate the total deposition amount of ^{137}Cs at the surface of the North Pacific from 170°E to 230°E in March.

We reported that WSPEEDI-DB would regionally underestimate the deposition density of ^{137}Cs in the North Pacific. Here, for the result of OCN_T20, we quantitatively estimated shortage deposition amounts (Bq) of ^{137}Cs required to improve the underestimation of ^{137}Cs concentrations in the sea surface water for the areas of 150°E−160°E and 170°E−230°E of the North Pacific. Table 5 shows the *Bias* values obtained from ^{137}Cs concentrations in the sea surface water from ATM-M_T20 and the measurement, and the deposition amounts (Bq) of ^{137}Cs used in OCN_T20. For 150°E−160°E, the *Bias* value was calculated as −0.18 from Eq. (2). Because the deposition amount of ^{137}Cs in this longitude zone on April 1, 2011, was 0.98 PBq, the shortage amount of ^{137}Cs deposition to set the *Bias* value to zero was roughly calculated as 0.50 PBq (Table 5). Similarly, the shortage amounts of ^{137}Cs deposition for the areas of 170°E−180°E, 180°E−190°E and 190°E−200°E were calculated as 0.54 PBq, 0.21 PBq and 0.10 PBq, respectively. When

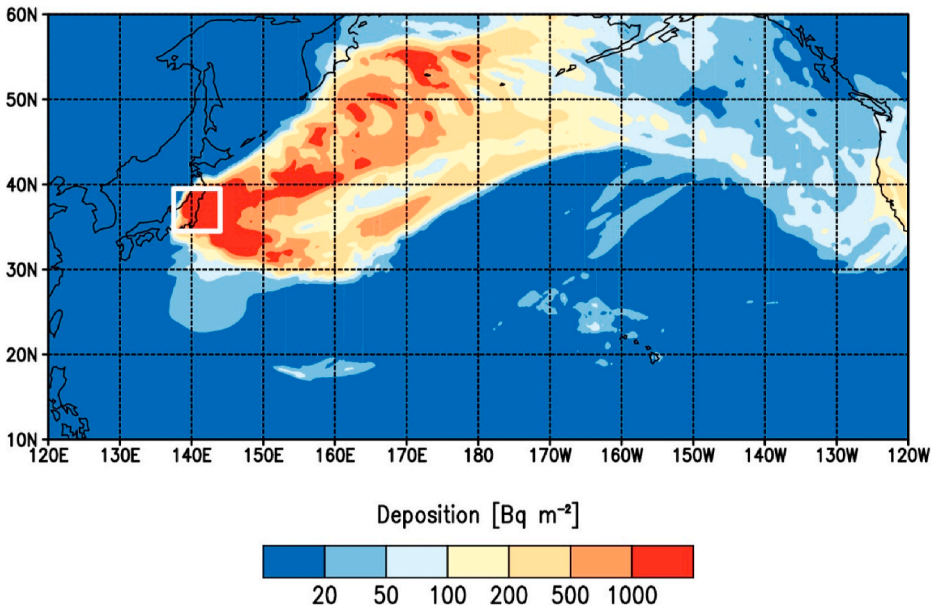

Fig. 10. The horizontal distribution of the deposition density (Bq m^{-2}) of ^{137}Cs. The amount of ^{137}Cs deposition was accumulated from March 11 to 31, 2011. The ^{137}Cs deposition was obtained from ATM-M_T20 (Table 3) and used in OCN_T20 (Table 4). The area surrounded by white lines (except for the area of ocean) includes the monitoring area of MEXT (2012). Blue (put in the most left) and red (put in the most right) of the color bar means the deposition density from 0 to 20 Bq m^{-2} and more than 1000 Bq m^{-2}, respectively. (For interpretation of the references to color in this figure legend, the reader is referred to the Web version of this article.)

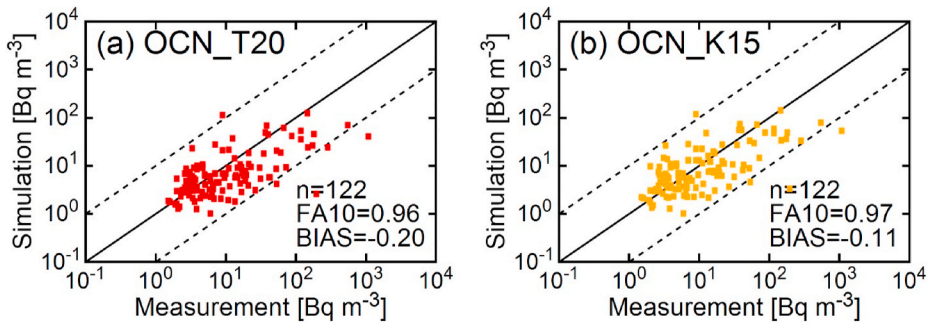

Fig. 11. A scatter plot of ^{137}Cs concentrations (Bq m^{-3}) in the sea surface water obtained from (a) OCN_T20 and (b) OCN_K15, compared with measurements reported by Aoyama et al. (2013). The zones between the dashed lines describe the area satisfying with a factor of 10 (*FA10*). Because the fallout of ^{137}Cs attributed to atomic weapons tests in the 20th century was not considered in the simulation, 1 Bq m^{-3} of background levels by Aoyama et al. (2006) was added to simulated ^{137}Cs concentrations in the sea surface water.

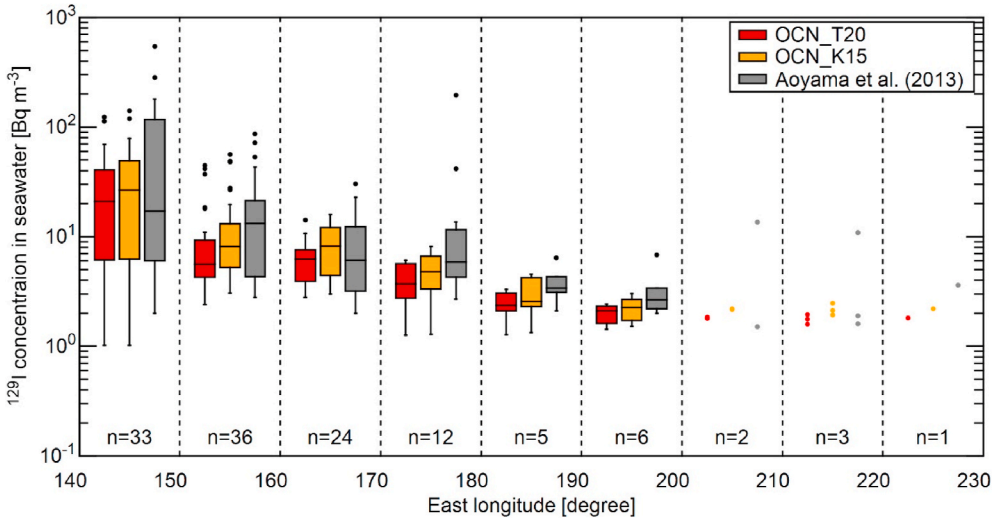

Fig. 12. Box plots of ^{137}Cs concentrations in the sea surface water for each longitude. The orange and gray boxes show the ^{137}Cs concentrations obtained from OCN_T20 and OCN_K15 and measurements reported by Aoyama et al. (2013), respectively. The boxes show the 25th–75th percentile of ^{137}Cs concentrations in the sea surface water, and the horizontal bars in the boxes are median values of ^{137}Cs concentration. *n* is the number of the ^{137}Cs measurement data. Because the fallout of ^{137}Cs attributed to atomic weapons tests in the 20th century was not considered in the simulation, 1 Bq m^{-3} of background level by Aoyama et al. (2006) was added to simulated ^{137}Cs concentrations in the sea surface water. (For interpretation of the references to color in this figure legend, the reader is referred to the Web version of this article.)

ignoring the latitudes east of 200°E where the number of comparing data was small (Fig. 11), if the above-estimated amounts of ^{137}Cs are further deposited in ATM-M_T20, the underestimation of ^{137}Cs concentrations in the sea surface water in the North Pacific can be modified. The possibility of this deposition occurring is discussed in Section 3.4.

3.4. Possibility of improving ^{137}Cs concentrations

In Section 3.3, we estimated the deposition amounts of ^{137}Cs required for improving underestimated concentrations of ^{137}Cs in the sea surface water. In this section, to confirm the possibility of improvement in the deposition, we investigate the long-range

Table 5
The *Bias* values for ^{137}Cs concentrations (Bq m^{-3}) in the sea surface water for longitude bands where the ^{137}Cs concentrations were underestimated by SEA-GEARN-FDM, and shortage deposition amounts of ^{137}Cs (PBq) required to improve the underestimation.

Longitude band[a] (°E)	*Bias*[b]	Deposition (PBq)	
		Simulation	Shortage[c]
150–160	−0.18	0.98	0.50
170–180	−0.28	0.59	0.54
180–190	−0.28	0.24	0.21
190–200	−0.23	0.15	0.10

[a] Longitude band from 200°E to 230°E is not shown because the number of comparing data is small.

[b] *Bias* is calculated using Eq. (2) from the results of OCN_T20 and the measurements reported by Aoyama et al. (2013). The fallout of ^{137}Cs attributed to global atomic weapons tests in the 20th century was not considered in the simulation. When calculating *Bias*, 1 Bq m^{-3} of background level by Aoyama et al. (2006) was subtracted from the measurements.

[c] When the values of *Bias* and simulated deposition are X and Y, respectively, the shortage amount is calculated as $(10^{-X} - 1) \times Y$.

atmospheric transport of ^{137}Cs in the simulation and discuss about the relationship between the behaviors of the ^{137}Cs plume and its deposition based on the precipitation distribution discussed in Section 3.1. Fig. 13 shows the horizontal distribution of daily-mean ground-level air concentrations (Bq m^{-3}) of ^{137}Cs from March 15 to 31, 2011 by ATM-M_T20. The boxed areas in Fig. 13 are the same as X and Y in Fig. 5 and are drawn at dates when the area-averaged daily precipitation by WRF was underestimated as more than 1 mm smaller than the measurement. From March 15 to 18, the ^{137}Cs plume, which was released from March 12 to 14, passed the X (Fig. 13a and b) and Y (Fig. 13d) areas and reached the eastern North Pacific and North America continent by March 20. From this spatiotemporal progress of the ^{137}Cs plume released from March 12 to 14, the overestimation of air concentrations of ^{137}Cs for CAP14 and USP70 of the IMS stations from March 19 to 21 (Fig. 8a and g) could be because of the ^{137}Cs plume that was largely unaffected by wet deposition.

In late March, although the air concentrations of ^{137}Cs from the measurement at the IMS stations in the eastern North Pacific were mostly less than 1.0×10^{-3} Bq m^{-3} (Fig. 8), for the simulation, air concentrations of ^{137}Cs more than 1.0×10^{-3} Bq m^{-3} (colored as yellow in Fig. 13e–p) were distributed in the area. The plume including high air-concentrations of ^{137}Cs, which was aerially released from FDNPS from March 18 to 20 (Fig. 13e and f), traveled through the Aleutian Islands (Fig. 13f–h) and came from north to south in the eastern North Pacific (Fig. 13i–p). The ^{137}Cs plume then moved from east to west in the low latitudes of the North Pacific. CAP14, USP70, USP77, and USP79 of the IMS stations, where the overestimation of air concentrations of ^{137}Cs was seen in late March (Fig. 8), were located on the pathway of this plume, showing that the plume determined the air concentrations of ^{137}Cs at these stations. Especially, the atmospheric release amount from March 18 to 20 was ~30 % of the total atmospheric released amount of ^{137}Cs from FDNPS in March 2011, and the influence on the deposition amount of ^{137}Cs underestimated in the simulation would be large. Because the above-mentioned plume passed through areas where precipitation was underestimated (plume distributed in the western part of North Pacific, colored as red in Fig. 13k–m), the overestimation of air concentrations of ^{137}Cs at these stations for late March can be attributed to the plume being unaffected by wet deposition. Furthermore, the plume which determined the air concentrations of ^{137}Cs for CAP14, USP70, USP77, and USP79 passed through the high latitudes of the North Pacific more than 45°N (Fig. 13e–j). In the high latitudes, while the simulated precipitation was not validated because of the low accuracy of the reanalysis product, the wet deposition in the high latitudes could also affect the air concentrations of ^{137}Cs for CAP14, USP70, USP77, and USP79.

We showed that the simulated ^{137}Cs plume, which influenced the overestimation of air concentrations of ^{137}Cs at the IMS stations, was sourced from the atmospheric release on March 12–14 and 18–20. The total amount of aerially released ^{137}Cs during these periods was 4.56 PBq (Terada et al., 2020a). From the atmospheric dispersion simulation using WSPEEDI-DB with the atmospheric release of ^{137}Cs only for the above periods, 3.14 PBq out of the ^{137}Cs released on March 12 to 14 and 18 to 20 was removed from the atmosphere by deposition in March 2011. This means that 1.42 PBq of ^{137}Cs existed in the atmosphere at the end of March 2011. Of the amount of 1.42 PBq, 1.36 PBq of ^{137}Cs was attributed to the release from March 18 to 20. On the other hand, we estimated the shortage amount of ^{137}Cs deposition from 150°E to 160°E and 170°E to 200°E as 1.35 PBq = 0.50 + 0.54 + 0.21 + 0.10 (Table 5). In Section 3.3.1, we showed that the simulated deposition amount of ^{137}Cs on the land area of Japan was underestimated. This underestimation possibly affected the simulated results over the ocean. However, the shortage of ^{137}Cs deposition amount over the ocean would not be significantly influenced by it because the ^{137}Cs deposition on land area mainly occurred by March 15. Therefore, the underestimated concentrations of ^{137}Cs in the sea surface water can be reasonably improved by more realistic precipitation. In addition, the estimated shortage amount of 1.35 PBq is almost comparable with the remained amount of ^{137}Cs by the release from March 18 to 20 (1.36 PBq). The comparable amounts mean that air concentrations of ^{137}Cs at CAP14, USP70, USP77, and USP79 in late March 2011 would become more than 1 order of magnitude lower than this study, if the shortage amount of ^{137}Cs is assumed to deposite to the ocean. Therefore, also the overestimation of air concentrations of ^{137}Cs at these stations could be improved as well as the concentrations in the sea water.

When improving the air concentrations of ^{137}Cs overestimated in the North Pacific by more realistic precipitation over the ocean, air concentrations of ^{137}Cs in the other regions might be different from the simulation result of this study. To discuss the influence on other regions by the improvement of the air concentrations in the North Pacific, we investigated the atmospheric transport of ^{137}Cs in the Northern Hemisphere. Fig. 14 shows the horizontal distribution of daily-mean ground-level air concentrations (Bq m^{-3}) of ^{137}Cs obtained from ATM-P_T20. Large amounts of ^{137}Cs were released from FDNPS into the atmosphere from March 12 to 14 and were widely dispersed in the Northern Hemisphere via the North Pacific, contributing mostly to the air concentrations of ^{137}Cs at the IMS stations plotted in Fig. 14. Here, to confirm quantitatively the impact of the release from March 12 to 14 on air concentrations of ^{137}Cs, the contribution rate $\Gamma_{M12\text{-}14}$ (%) for each station from March 12 to April 1, 2011 was calculated as in Eq. (3).

$$\Gamma_{M12-14} = \frac{C_{M12-14}}{C_{ATM-P\_T20}} \times 100 \quad (3)$$

where $C_{M12\text{-}14}$ and $C_{ATM\text{-}P\_T20}$ show the daily-mean ground-level air concentration (Bq m^{-3}) of ^{137}Cs simulated using only the release from March 12 to 14 and that by ATM-P_T20, respectively. The values of $\Gamma_{M12\text{-}14}$ were calculated for IMS stations after March 12 and are tabulated in Table 6.

The widely dispersing plume passed the areas where the precipitation was underestimated by WSPEEDI-DB on March 16 and 18 (Fig. 14a and b) and reached Europe via North America and the North Atlantic by March 21 with air concentrations of ^{137}Cs more than 1.0×10^{-6} Bq m^{-3} (Fig. 14b and c). For days from March 12 to 21 when the air concentrations exceeded 1.0×10^{-6} Bq m^{-3}, the values of $\Gamma_{M12\text{-}14}$ for the IMS stations in North America were 83 % (CAP17), 96–99 % (USP74), and 98–99 % (USP75), respectively (Table 6). The release from March 12 to 14 was the largest contributor to the air concentrations at these IMS stations. The impact of deposition of ^{137}Cs attributing to the release from March 12 to 14 due to more realistic precipitation on air concentrations of ^{137}Cs in these stations would be small because airborne ^{137}Cs released from March 12 to 14 was mostly removed from the atmosphere in the

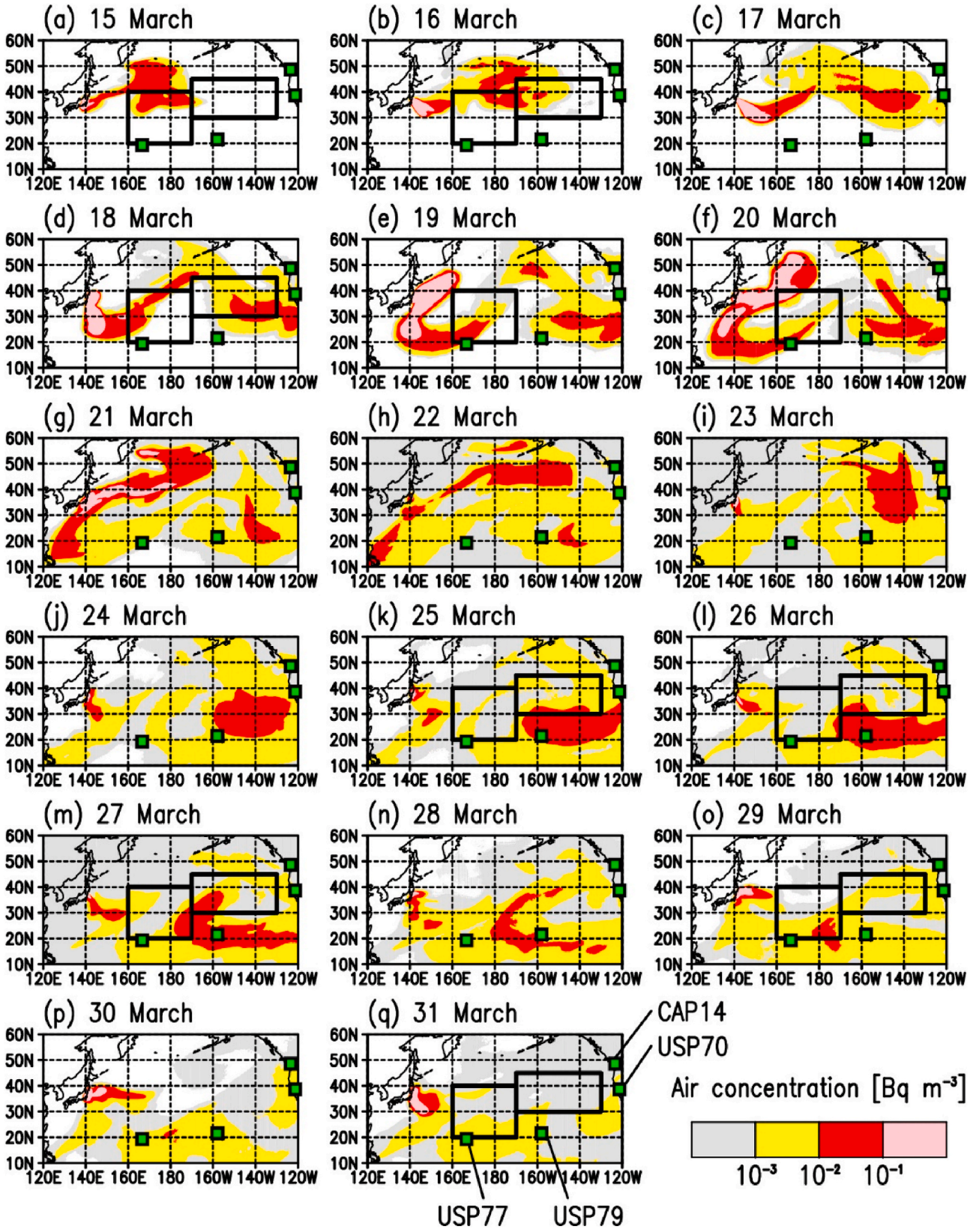

Fig. 13. Horizontal distribution of daily-mean ground-level air concentrations of ^{137}Cs (Bq m^{-3}) by ATM-M_T20. The boxed areas in the figures are the same as X and Y in Fig. 5 and were drawn on the day when the area-averaged daily precipitation by WRF was underestimated as more than 1 mm smaller than the measurement. The green squares in the figures show the locations of CAP14, USP70, USP77, and USP79. In this comparison, we used the simulated air concentrations at the bottom layer with the 20 m thickness. Light gray (put in the most left) and pink (put in the most right) of the color bar means the air concentration from 1.0×10^{-6} to 1.0×10^{-3} Bq m^{-3} and more than 0.1 Bq m^{-3}, respectively. The air concentration lower than 1.0×10^{-6} Bq m^{-3} is not colored in the figure. (For interpretation of the references to color in this figure legend, the reader is referred to the Web version of this article.)

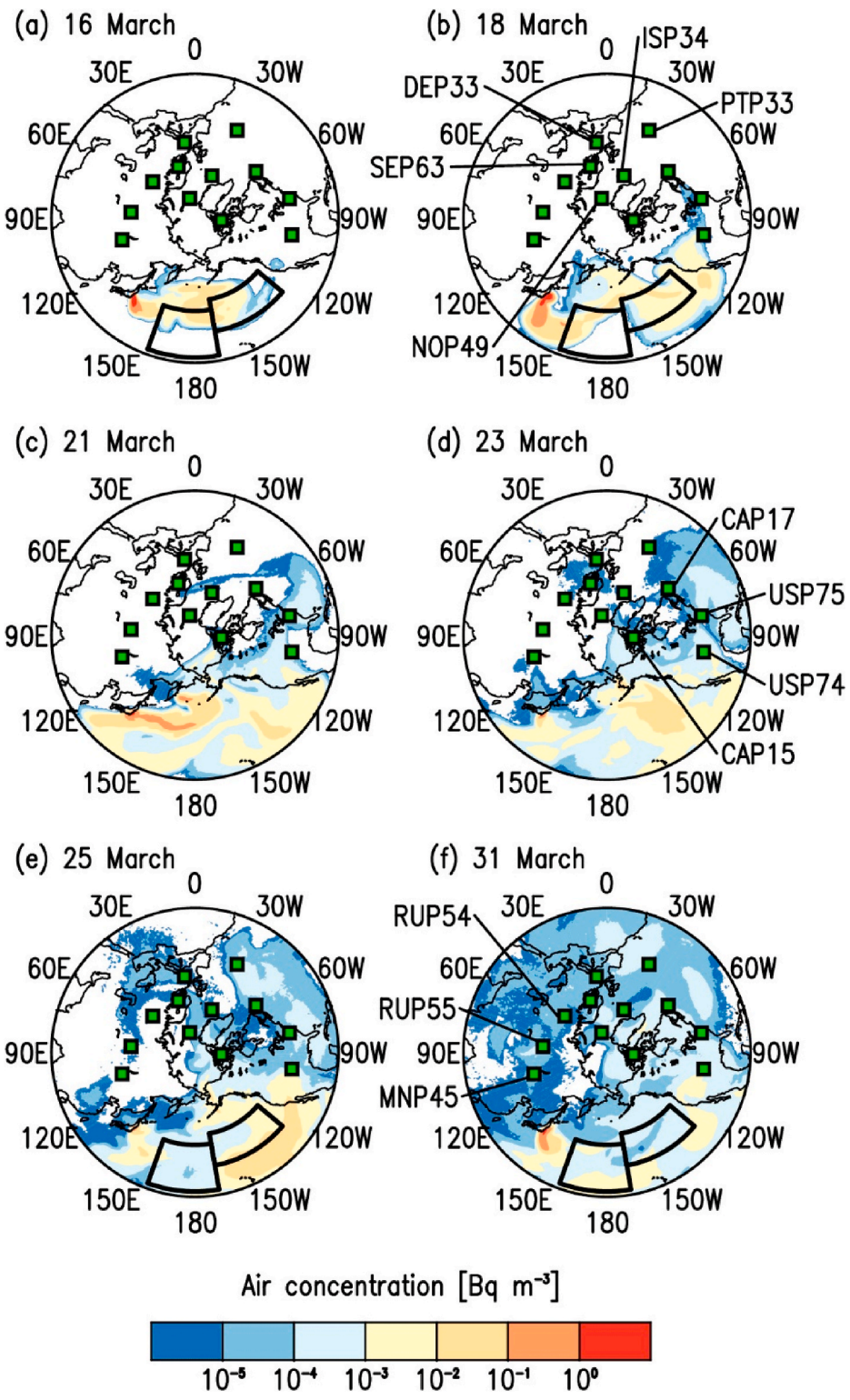

Fig. 14. Horizontal distribution of daily-mean ground-level air concentrations of ^{137}Cs (Bq m^{-3}) on (a) 15 March, (b) 17 March, (c) 21 March, (d) 23 March, (e) 24 March, and (f) 30 March, obtained from ATM-P_T20. The boxed areas in Fig. 14a, showing the same areas as the boxes of X and Y in Fig. 5, indicate where the area-averaged daily precipitation simulated by WRF was underestimated more than 1 mm than the measurement. The green squares in the figures show the locations of CTBTO stations in Table 1. In this comparison, we used the simulated air concentrations at the bottom layer with the 20 m thickness. Blue (put in the most left) and red (put in the most right) of the color bar means the air concentration from 1.0×10^{-6} to 1.0×10^{-5} Bq m^{-3} and more than 1 Bq m^{-3}, respectively. The air concentration lower than 1.0×10^{-6} Bq m^{-3} is not colored in the figure. (For interpretation of the references to color in this figure legend, the reader is referred to the Web version of this article.)

simulation of this study. Of the residual amount in the atmosphere (1.42 PBq), only 0.06 PBq was attributed to the ^{137}Cs plume released from March 12 to 14. This amount shows that the deposition of ^{137}Cs aerially released from March 12 to 14 would not majorly contribute to the improvement. Therefore, even if airborne ^{137}Cs released from March 12 to 14 is further deposited, the high reproducibility of air concentrations of ^{137}Cs for Other regions (Fig. 7b) would be preserved.

A part of the plume moved to Europe via the Arctic region (Fig. 14c–e). In late March, the plume moved easterly from Europe and was broadly distributed over Russia and Asia (Fig. 14d–f). For stations in Europe, Russia and Asia regions, the values of $\Gamma_{M12\text{-}14}$ after March 21 ranged from 81 to 100 % (CAP15), 40–98 % (DEP33), 66–100 % (ISP34), and 59–100 % (PTP53), respectively (Table 6). These high values of $\Gamma_{M12\text{-}14}$ for these stations were obtained from the air concentrations from March 21 to 29. This result shows that the release from March 12 to 14 mainly influenced on the air concentrations of ^{137}Cs at these stations. On the other hand, several stations in the regions showed widely-ranged values of $\Gamma_{M12\text{-}14}$: 8–100 % (NMP45), 2–100 % (NOP49),

Table 6
Contribution rate (%) of ^{137}Cs aerially released from March 12–14 and 18–20 to air concentrations of ^{137}Cs at IMS stations in Pacific and other regions. The contribution rate is calculated from Eq. (3).

Station code	Region[a]	Country	Contribution rate (%)		
			$\Gamma_{M12\text{-}14}$		$\Gamma_{M18\text{-}20}$
			March 12–21	March 21–31	March 30–31
CAP17	Pacific	Canada	83		
USP74	Pacific	USA	96–99		
USP75	Pacific	USA	98–99		
CAP15	Other	Canada		81–100	
DEP33	Other	Germany		40–98	
ISP34	Other	Iceland		66–100	
PTP53	Other	Portugal		59–100	
MNP45	Other	Mongolia		8–100	19–61
NOP49	Other	Norway		2–100	91–95
RUP54	Other	Russia		28–100	39–54
RUP59	Other	Russia		18–100	29–35
SEP63	Other	Sweden		29–100	55–58

[a] The definition of region is shown in Table 1.

28–100 % (RUP54), 18–100 % (RUP59) and 29–100 % (SEP63) (Table 6). The low values of $\Gamma_{M12\text{-}14}$ were seen after March 30. As well as the estimate of the impact of the release from March 12 to 14, when calculating the contribution rate regarding the release from March 18 to 20 using Eq. (3), the values of $\Gamma_{M18\text{-}20}$ after March 30 ranged from 19 to 61 % (NMP45), 91–95 % (NOP49), 39–54 % (RUP54), 29–35 % (RUP59), and 55–58 % (SEP63), respectively (Table 6). These ranges indicate that the air concentrations of ^{137}Cs at these stations after March 30 were largely affected by the release from March 18 to 20. Here, using a statistic score of *FA10*, we evaluated the reproducibility of air concentrations of ^{137}Cs where the release from March 18 to 20 was ignored. From the air concentrations of ^{137}Cs simulated by WSPEEDI-DB without the release from March 18 to 20, the value of *FA10* for the air concentrations of ^{137}Cs at the stations (NMP45, NOP49, RUP54, RUP59, and SEP63) was calculated as 0.77. This value demonstrates that the air concentrations would be acceptably consistent to the measurement without considering the release from March 18 to 20. Therefore, the reasonable reproducibility of air concentrations of ^{137}Cs at the IMS stations of Europe, Arctic, Russia, and Asia would be still remained, even if a further deposition occurs due to more realistic precipitation.

4. Conclusions

In this study, we investigated the validity of the source term of ^{137}Cs for the FDNPS accident estimated by local-scale atmospheric dispersion simulations (Terada et al., 2020a), to reproduce the hemispheric-scale atmospheric dispersion of ^{137}Cs. The atmospheric dispersion simulations were conducted using the atmospheric-dispersion database system WSPEEDI-DB developed at JAEA (Terada et al., 2020b). The meteorological fields required in the atmospheric dispersion simulations were

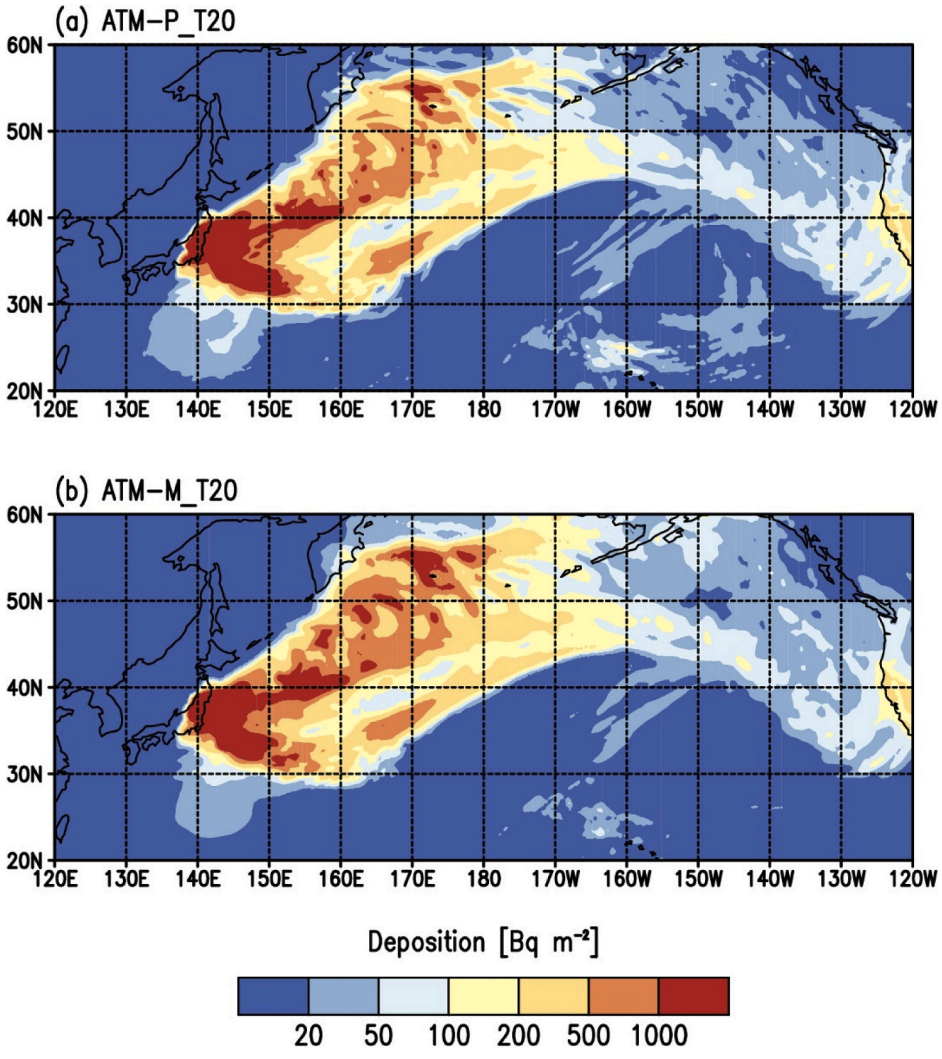

Fig. A.1. Horizontal distribution of the deposition density (Bq m^{-2}) of ^{137}Cs on the ground and sea surface obtained from (a) ATM-P_T20 and (b) ATM-M_T20. The deposition amount of ^{137}Cs is accumulated from March 11 to 31, 2011. The area where the calculation domains of both simulations completely overlap is shown in the figures as a comparison area. Blue (put in the most left) and red (put in the most right) of the color bar means the deposition density from 0 to 20 Bq m^{-2} and more than 1000 Bq m^{-2}, respectively.

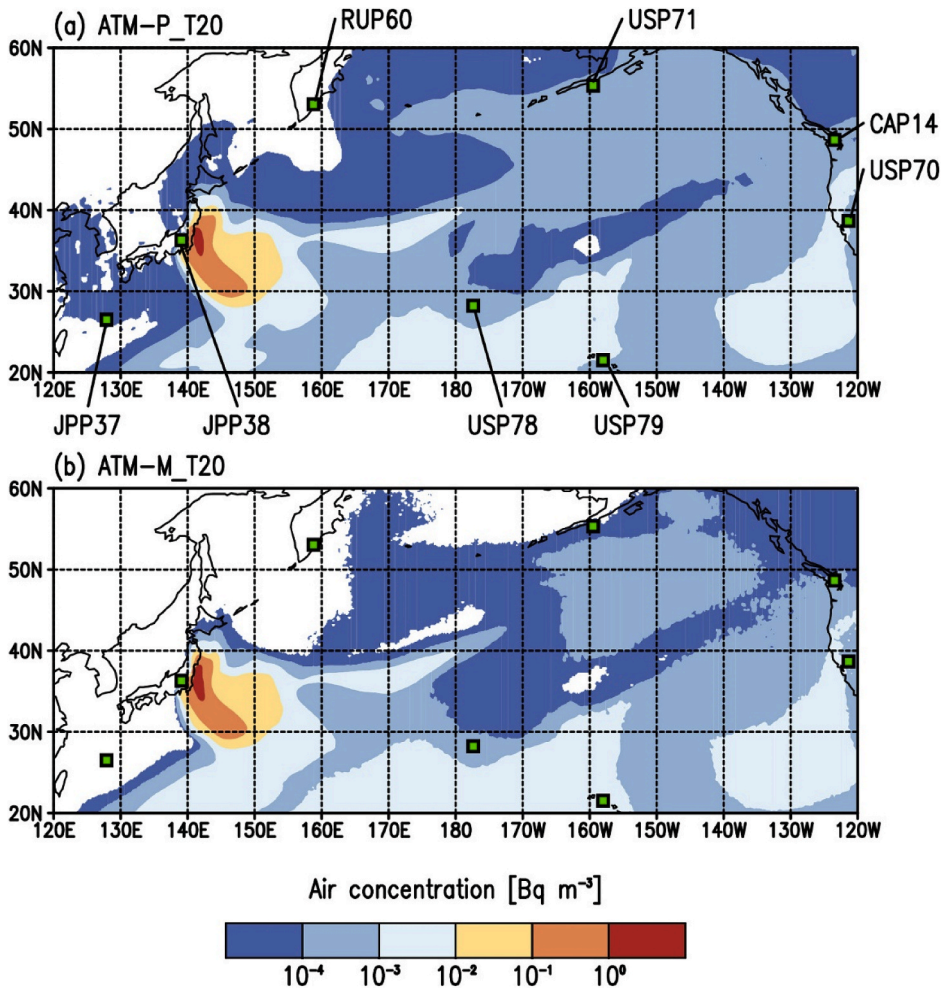

Fig. A.2. Horizontal distribution of daily-mean ground-level air concentrations (Bq m^{-3}) of ^{137}Cs on March 31, 2011, obtained from (a) ATM-P_T20 and (b) ATM-M_T20. The area where the calculation domains of both simulations completely overlap is shown in the figures as a comparison area. The green squares in the figures show the locations of CAP14, JPP37, JPP38, RUP60, USP70, USP71, USP77 and USP79. In this comparison, we used the simulated air concentrations at the bottom layer with the 20 m thickness. Blue (put in the most left) and red (put in the most right) of the color bar means the air concentration from 1.0×10^{-6} to 1.0×10^{-4} Bq m^{-3} and more than 1 Bq m^{-3}, respectively. The air concentration lower than 1.0×10^{-6} Bq m^{-3} is not colored in the figure.

calculated using a meteorological model WRF and transport and deposition of ^{137}Cs were calculated using the atmospheric dispersion model GEARN in the system. The result of the simulation demonstrated enough reproducibility of air concentrations of ^{137}Cs at the IMS stations, with good scores of statistics. The score obtained from the simulation result using the source term by Terada et al. (2020a) was higher than that by Katata et al. (2015). This analysis result indicates that the hemispheric-scale atmospheric dispersion of ^{137}Cs in the simulation using the source term by Terada et al. (2020a) is more reasonable than that by Katata et al. (2015). In addition, the deposition amount of ^{137}Cs over land area of Japan by the hemispheric-scale atmospheric dispersion simulations using the source term by Terada et al. (2020a) was agreement to the airborne monitoring, as well as the regional dispersion simulation by Terada et al. (2020a). This quantitative accordance evidences that the enough availability of the source term by Terada et al. (2020a) to local to large-scale atmospheric dispersion simulations. Furthermore, the ^{137}Cs deposition by WSPEEDI-DB using the source term by Terada et al. (2020a) was validated by comparing ^{137}Cs concentrations in the sea surface water with measurement data reported by Aoyama et al. (2013). The ^{137}Cs concentrations in the sea surface water were simulated by SEA-GEARN-FDM, an oceanic dispersion model developed at JAEA. In the oceanic dispersion simulation, the deposition flux of ^{137}Cs obtained from the atmospheric dispersion simulation using the source term by Terada et al. (2020a) in this study was used as input data from the atmosphere to oceans. While the ^{137}Cs concentration in the sea surface water by SEA-GEARN-FDM was statistically good, the result of the simulation were regionally underestimated. We specified that this underestimation would be attributed to the small wet deposition of ^{137}Cs because of underestimated precipitation over the North Pacific. Underestimating the deposition density of ^{137}Cs would be improved by more realistic precipitation over the North Pacific with the improvement of overestimated air concentrations of ^{137}Cs in some measurements, showing that the source term by Terada et al. (2020a) is valid in large-scale atmospheric dispersion of ^{137}Cs. The results indicate that WSPEEDI-DB using the source term by Terada et al. (2020a) can widely address scales from local to hemisphere atmospheric dispersion of ^{137}Cs because of the FDNPS accident.

Declaration of competing interest

The authors declare that they have no known competing financial interests or personal relationships that could have appeared to influence the work reported in this paper.

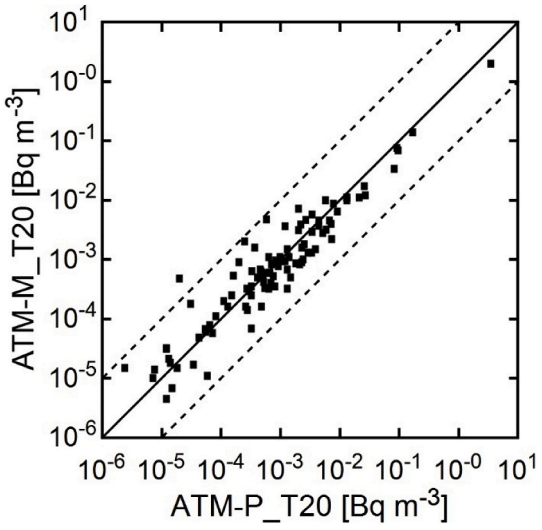

Fig. A.3. Scatter plots of daily-mean ground-level air concentrations (Bq m^{-3}) of ^{137}Cs between 12 and 31 March obtained from ATM-P_T20 and ATM-M_T20. The plotted air concentrations are taken from CAP14, JPP37, JPP38, RUP60, USP70, USP71, USP77 and USP79 (Fig. A2). The zones between the dashed lines describe the area satisfying with a factor of 10 (*FA10*). In this comparison, we used the simulated air concentrations at the bottom layer with the 20 m thickness.

Acknowledgments

The authors thank the station operators of the IMS stations, which provide useful measurement data. The authors thank Ms. Nemoto of Visible Information Center, Inc. for the technical support in conducting the oceanic dispersion simulation. This study was supported by the Environment Research and Technology Development Fund (JPMEERF20181002) of Environmental Restoration and Conservation Agency of Japan.

Appendix A. Consistency of two atmospheric dispersion simulations

In this study, to discuss the validity of the source term to reproduce the hemispheric-scale atmospheric dispersion of ^{137}Cs, we used the results of two simulations, ATM-P_T20 and ATM-M_T20. When analyzing the results and discussing the validity of the source term, consistency between the simulations is required. Therefore, we confirmed it in this section. Figure A1 shows the horizontal distribution of the deposition density (Bq m^{-2}) of ^{137}Cs accumulated from March 11 to 31, 2011, obtained by ATM-P_T20 and ATM-M_T20. The horizontal distribution of the deposition amounts by these simulations was similar. From the result of ATM-P_T20, the total deposition amount of ^{137}Cs in the entire area of Fig. A1 was calculated as 7.9 PBq. This amount was consistent with 7.7 PBq from that of ATM-M_T20, although the amount by ATM-P_T20 was slightly larger than that by ATM-M_T20. Furthermore, we show the horizontal distribution of air concentrations (Bq m^{-3}) of ^{137}Cs on March 31 in Fig. A2, which is the same date as Fig. A1, as an example for the comparison regarding the air concentration of ^{137}Cs. Overall, the spatial pattern of air concentrations by ATM-P_T20 was consistent with that by ATM-M_T20, although the spatial pattern by ATM-P_T20 was different from that by ATM-M_T20 near the north and west boundaries of the calculation domain of ATM-M_T20. This difference near the boundaries could be because in ATM-M_T20, once tracer particles move out of the calculation domain, the tracer particles cannot return to the calculation domain across boundaries. Activities of airborne ^{137}Cs that left in the entire Fig. A2 area were calculated as 2.1 PBq for ATM-P_T20 and 2.3 PBq for ATM-M_T20, from the total amount of the atmospheric released ^{137}Cs by Terada et al. (2020a), and 7.9 PBq and 7.7 PBq of the deposition amounts of ^{137}Cs by ATM-P_T20 and ATM-M_T20 in Fig. A1. The difference in activities between the two simulations was 0.2 PBq, corresponding to ~10 % of 2.1 PBq and 2.3 PBq of the activities. This result shows the uncertainty of atmospheric dispersion simulations of ^{137}Cs because of the setup of simulation domains of this study. This uncertainty could influence on the underestimation of air concentrations of ^{137}Cs in the Other region. Considering the good consistency of the deposition amounts of ^{137}Cs between ATM-P_T20 and ATM-M_T20, the impact of the difference near the boundaries on the consistency of hemispheric-scale atmospheric dispersion of ^{137}Cs between ATM-P_T20 and ATM-M_T20 would be small. In the comparison area in Fig. A2, several IMS stations (CAP14, JPP37, JPP38, RUP60, USP70, USP71, USP77 and USP79) were included, and thus we also compared the air concentrations of ^{137}Cs at these stations. Figure A3 shows the scatter plots of daily-mean ground-level air concentrations (Bq m^{-3}) of ^{137}Cs of March 12–31 from the results of ATM-P_T20 and ATM-M_T20. The air concentrations of ^{137}Cs at these simulations showed strong correlations, with a high score of $FA10 = 0.89$. These results support that the atmospheric dispersion of ^{137}Cs by ATM-P_T20 was reasonably consistent with that by ATM-M_T20, showing that we can analyze the results from ATM-P_T20 and ATM-M_T20 coherently.

References

Achim, P., Monfort, M., Le Petit, G., Gross, P., Douysset, G., Taffary, T., Blanchard, X., Moulin, C., 2014. Analysis of radionuclide releases from the Fukushima Dai-ichi nuclear power plant accident part II. Pure Appl. Geophys. 171, 645–667. https://doi.org/10.1007/s00024-012-0578-1.

Aoyama, M., Hirose, K., Igarashi, Y., 2008. Re-construction and updating our understanding on the global weapons tests ^{137}Cs fallout. J. Environ. Monit. 8, 431–438. https://doi.org/10.1039/b512601k.

Aoyama, M., Uematsu, M., Tsumune, D., Hamajima, Y., 2013. Surface pathway of radioactive plume of TEPCO Fukushima NPP1 released ^{134}Cs and ^{137}Cs. Biogeosciences 10, 3067–3078. https://doi.org/10.5194/bg-10-3067-2013.

Betts, A.K., Miller, M.J., 1993. The Betts–Miller scheme. The representation of cumulus convection in numerical models. Meteor. Monogr. 46, 107–121. Amer. Meteor. Soc.

Chino, M., Nakayama, H., Nagai, H., Terada, H., Katata, G., Yamazawa, H., 2011. Preliminary estimation of release amounts of ^{131}I and ^{137}Cs accidently discharged from the Fukushima Daiichi nuclear power plant into atmosphere. J. Nucl. Sci. Technol. 48, 1129–1134. https://doi.org/10.1080/18811248.2011.9711799.

Chino, M., Terada, H., Nagai, H., Katata, G., Mikami, S., Torii, T., Saito, K., Nishizawa, Y., 2016. Utilization of ^{134}Cs/^{137}Cs in the environment to identify the reactor units that caused atmospheric releases during the Fukushima Daiichi accident. Sci. Rep. 6, 31376. https://doi.org/10.1038/srep31376.

Accessed on 21 January, 2021 CTBTO (Comprehensive Nuclear-Test-Ban Treaty Organization), 2011, Preparatory Commission. Fukushima-related Measurements by the CTBTO. http://www.ctbto.org/press-centre/highlights/2011/fukushima-related-measurements-by-the-ctbto.

Draxler, R.R., Rolph, G.D., 2012. Evaluation of the transfer coefficient matrix (TCM) approach to model the atmospheric radionuclide air concentrations from Fukushima. J. Geophys. Res. 117, D05107 https://doi.org/10.1029/2011JD017205.

Dudhia, J., 1989. Numerical study of convection observed during the winter monsoon experiment using a mesoscale two-dimensional model. J. Atmos. Sci. 46, 3077–3107, 10.1175/1520-0469(1989)046<3077: NSOCOD>2.0.CO;2.

Katata, G., Nagai, H., Terada, H., Chino, M., 2012a. Numerical reconstruction of high dose rate zones due to the Fukushima Dai-ichi Nuclear Power Plant accident. J. Environ. Radioact. 111, 2–12. https://doi.org/10.1016/j.jenvrad.2011.09.011.

Katata, G., Ota, M., Terada, H., Chino, M., Nagai, H., 2012b. Atmospheric discharge and dispersion of radionuclides during the Fukushima Dai-ichi Nu-clear Power Plant accident. Part I: source term estimation and local-scale atmospheric dispersion in early phase of the accident. J. Environ. Radioact. 109, 103–113. https://doi.org/10.1016/j.jenvrad.2012.02.006.

Katata, G., Chino, M., Kobayashi, T., Terada, H., Ota, M., Nagai, H., Kajino, M., Draxler, R., Hort, M., Malo, A., Torii, T., Sanada, Y., 2015. Detailed source term estimation of the atmospheric release for the Fukushima Daiichi Nuclear Power Station accident by coupling simulations of an atmospheric dispersion model with an improved deposition scheme and oceanic dispersion model. Atmos. Chem. Phys. 15, 1029–1070. https://doi.org/10.5194/acp-15-1029-2015.

Kawamura, H., Kobayashi, T., Furuno, A., 2011. Preliminary numerical experiments on oceanic dispersion of ^{131}I and ^{137}Cs discharged into the ocean because of the Fukushima Daiichi Nuclear Power Plant Disaster. J. Nucl. Sci. Technol. 48, 1349–1356. https://doi.org/10.1080/18811248.2011.9711826.

Kawamura, H., Kobayashi, T., Furuno, A., Usui, N., Kamachi, M., 2014. Numerical simulation on the long-term variation of radioactive cesium concentration in the North Pacific due to the Fukushima disaster. J. Environ. Radioact. 136, 64–75. https://doi.org/10.1016/j.jenvrad.2014.05.005.

Kawamura, H., Furuno, A., Kobayashi, T., T, Nakayama, T., Ishikawa, Y., Miyazawa, Y., Usui, N., 2017. Oceanic dispersion of Fukushima-derived Cs-137 simulated by multiple oceanic general circulation models. J. Environ. Radioact. 180, 36–58. https://doi.org/10.1016/j.jenvrad.2017.09.020.

Kobayashi, T., Nagai, H., Chino, M., Kawamura, H., 2013. Source term estimation of atmospheric release due to the Fukushima Dai-ichi Nuclear Power Plant accident by atmospheric and oceanic dispersion simulations. J. Nucl. Sci. Technol. 50, 255–264. https://doi.org/10.1080/00223131.2013.772449.

Kubota, T., Aonashi, K., Ushio, T., Shige, S., Takayabu, Y.N., Kachi, M., Arai, Y., Tashima, T., Masaki, T., Kawamoto, N., Mega, T., Yamamoto, M.K., Hamada, A., Yamaji, M., Liu, G., Oki, R., 2020. Global Satellite Mapping of Precipitation (GSMaP) Products in the GPM Era, Satellite Precipitation Measurement. Springer. https://doi.org/10.1007/978-3-030-24568-9_20.

Maki, T., 2015. Emission source estimation by an inverse model. Contribution of JMA to the WMO Technical Task Team on Meteorological Analyses for Fukushima Daiichi Nuclear Power Plant Accident and Relevant Atmospheric Transport Modelling at MRI, Technical Reports of the Meteorological Research Institute No.76. Meteorological Research Institute, Tsukuba, pp. 150–153.

Mészáros, R., Leelőssy, A., Kovács, T., Lagzi, I., 2016. Predictability of the dispersion of Fukushima-derived radionuclides and their homogenization in the atmosphere. Sci. Rep. 6, 19915. https://doi.org/10.1038/srep19915.

MEXT (Ministry of Education, Culture, Sports Science and Technology), 2012. (i) Results of Airborne Monitoring Survey in Hokkaido and (ii) Revision to the Results of Airborne Monitoring Survey over the Eastern Part of Japan with Detailed Consideration of the Influence of Natural Radionuclides. https://radioactivity.nsr.go.jp/en/contents/6000/5188/24/203_e_0727_14.pdf. (Accessed 20 January 2021).

Mlawer, E.J., Taubman, S.J., Brown, P.D., Iacono, M.J., Clough, S.A., 1997. Radiative transfer for inhomogeneous atmosphere, RRTM, a validated correlated-k model for the long wave. J. Geophys. Res. 102, 16. https://doi.org/10.1029/97JD00237, 663–16,682.

Morrison, H., Curry, J.A., Khvorostyanov, V.I., 2005. A new double-moment microphysics parameterization for application in cloud and climate models. Part I: description. J. Atoms. Sci. 62 (6), 1665–1677. https://doi.org/10.1175/JAS3446.1.

Nakanishi, M., Niino, H., 2004. An improved Mellor–Yamada level-3 model with condensation physics: its design and verification. Boundary-Layer Meteorol. 112 (4), 1–31. https://doi.org/10.1023/B:BOUN.0000020164.04146.98.

Oura, Y., Ebihara, M., Tsuruta, H., Nakajima, T., Ohara, T., Ishimoto, M., Sawahata, H., Katsumura, Y., Nitta, W., 2015. A database of hourly atmospheric concentrations of radiocesium (^{134}Cs and ^{137}Cs) in suspended particulate matter collected in March 2011 at 99 air pollution monitoring stations in eastern Japan. J. Nucl. Radiochem. Sci. 15 (2), 15–26. https://doi.org/10.14494/jnrs.15.2_1.

Sarkar, T., Anand, S., Singh, K.-D., Tripathi, R.-M., Pradeepkumar, K.-S., Goto, D., Nakajima, T., 2017. Simulating long range transport of radioactive aerosols using a global aerosol transport model. Aerosol Air Qual. Res. 17, 2631–2642. https://doi.org/10.4209/aaqr.2017.01.0049.

Skamarock, W.-C., Klemp, J.-B., Dudhia, J., Gill, D.-O., Barker, D.-M., Duda, M.-G., Huang, X.-Y., Wang, W., Powers, J.-G., 2008. A Description of the Advanced Research WRF Version 3. National Center for Atmospheric Research, USA. NCAR/TN-475STR. doi.org/10.5065/D68S4MVH.

Smagorinsky, J., 1963. General circulation experiments with the primitive equation I the basic experiment. Mon. Weather Rev. 91, 99–164 doi.org/10.1175/1520-0493(1963)091<0099:GCEWTP>2.3.CO;2.

Stohl, A., Seibert, P., Wotawa, G., Arnold, D., Burkhart, J.-F., Eckhardt, S., Tapia, C., Vargas, A., Yasunari, T.-J., 2012. Xenon-133 and caesium-137 releases into the atmosphere from the Fukushima Dai-ichi nuclear power plant: determination of the source term, atmospheric dispersion, and deposition. Atmos. Chem. Phys. 12, 2313–2343. https://doi.org/10.5194/acp-12-2313-2012.

Terada, H., Chino, M., 2008. Development of an atmospheric dispersion model for accidental discharge of radionuclides with the function of simultaneous prediction for multiple domains and its evaluation by application to the Chernobyl nuclear accident. J. Nucl. Sci. Technol. 45, 920–931. https://doi.org/10.1080/18811248.2008.9711493.

Terada, H., Katata, G., Chino, M., Nagai, H., 2012. Atmospheric discharge and dispersion of radionuclides during the Fukushima Dai-ichi Nuclear Power Plant accident. Part II: verification of the source term and regional-scale atmospheric dispersion. J. Environ. Radioact. 112, 141–154. https://doi.org/10.1016/j.jenvrad.2012.05.023.

Terada, H., Nagai, H., Yamazawa, H., 2013. Validation of a Lagrangian atmospheric dispersion model against middle-range scale measurements of 85Kr concentration in Japan. J. Nucl. Sci. Technol. 50, 1198–1212. https://doi.org/10.1080/00223131.2013.840545.

Terada, H., Nagai, H., Tsuduki, K., Furuno, A., Kadowaki, M., Kakefuda, T., 2020a. Refinement of source term and atmospheric dispersion simulations of radionuclides during the Fukushima Daiichi Nuclear Power Station accident. J. Environ. Radioact. 213, 106104 https://doi.org/10.1016/j.jenvrad.2019.106104.

Terada, H., Nagai, H., Tanaka, A., Tsuduki, K., Kadowaki, M., 2020b. Atmospheric-dispersion database system that can immediately provide calculation results for various source term and meteorological conditions. J. Nucl. Sci. Technol. 57 (6), 745–754. https://doi.org/10.1080/00223131.2019.1709994.

Torii, T., Sugita, T., Okada, C.-E., Reed, M.-S., Blumenthal, D.-J., 2013. Enhanced analysis methods to derive the spatial distribution of ^{131}I deposition on the ground by airborne surveys at an early stage after the Fukushima Daiichi nuclear power plant accident. Health Phys. 105, 192–200. https://doi.org/10.1097/HP.0b013e318294444e.

Tsuruta, H., Oura, Y., Ebihara, M., Moriguchi, Y., Ohara, T., Nakajima, T., 2018. Time-series analysis of atmospheric radiocesium at two SPM monitoring sites near the Fukushima Daiichi Nuclear Power Plant just after the Fukushima accident on March 11, 2011. Geochem. J. 52, 103–121. https://doi.org/10.2343/geochemj.2.0520.

UNSCEAR (United Nations Scientific Committee on the Effects of Atomic Radiation), 2014. UNSCEAR 2013 Report: Sources, Effects and Risks of Ionizing Radiation, vol. I. United Nations, New York, p. 311.

Usui, N., Ishizaki, S., Fujii, Y., Yasuda, T., Kamachi, M., 2006. Meteorological Research Institute multivariate ocean variational estimation (MOVE) system: some early results. Adv. Space Res. 37, 806–822. https://doi.org/10.1016/j.asr.2005.09.022.

Winiarek, V., Bocquet, M., Saunier, O., Mathieu, A., 2012. Estimation of errors in the inverse modeling of accidental release of atmospheric pollutant: application to the reconstruction of the cesium-137 and iodine-131 source terms from the Fukushima Daiichi power plant. J. Geophys. Res. 117, D05122 https://doi.org/10.1029/2011JD016932.